POLITECNICO DI TORINO

Collegio di Ingegneria Chimica e dei Materiali

Master of Science Course
in Materials Engineering for Industry 4.0

Master of Science Thesis

Optimization of PEO coatings on magnesium alloys: towards a balance between biocompatible materials and durability for biomedical implants.



Supervisors:
Prof. Marjorie Olivier
Prof. Sara Ferraris

Co-supervisor:
Isis Tournay-Dufrenne

Candidate :
Sofia Vicquéry

Accademic Year 2025/2026

Abstract

Magnesium alloys are increasingly investigated for biodegradable biomedical implants due to their mechanical properties and biocompatibility. However, their high corrosion rate in physiological environments still represents a major limitation. In this work, AZ31 magnesium alloy was treated by Plasma Electrolytic Oxidation (PEO) followed by a phosphate post-conversion treatment to improve corrosion resistance and promote the incorporation of the anti-inflammatory drug Betamethasone Sodium Phosphate (BSP).

The phosphate conversion treatment was performed in a Na–P solution at pH 9 and 60 °C, investigating three immersion times (30 min, 1 h and 2 h). Morphological, chemical and electrochemical characterizations were carried out through SEM-EDS, XRD and Electrochemical Impedance Spectroscopy (EIS). The results showed that the 1 h treatment provided the most favourable balance between phosphate layer formation and preservation of the underlying PEO coating. In particular, the 30 min treatment produced a non-uniform phosphate deposition, while the 2 h treatment appeared to promote partial re-dissolution of the formed phosphate compounds.

Different BSP deposition strategies and solvents were investigated. Methanol-based deposition systems generally preserved the phosphate layer more effectively than aqueous-based systems, which frequently induced partial dissolution of the coating. SEM and EDS analyses suggested the possible presence of superficial deposited layers; although, the measured carbon contents remained lower than expected for a significant BSP incorporation. UV–Vis spectroscopy did not provide reliable quantitative evidence of BSP release, since the measured absorbance values remained close to the baseline and below the effective quantification range of the calibration curve throughout the immersion tests.

Overall, the results confirmed the beneficial effect of phosphate post-conversion treatments on the corrosion behaviour of PEO-coated AZ31 magnesium alloy, while highlighting the complexity of achieving stable BSP incorporation within the coating system. Further investigations employing more selective characterization techniques and alternative deposition strategies are required to better clarify the interactions between BSP, phosphate compounds and the PEO-modified surface.

Acknowledgements

An incredible journey is coming to an end, and I would like to thank all the people who have been part of it and supported me along the way.

First of all, I would like to thank my supervisor, Marjorie Olivier, for giving me the opportunity to carry out this Master's thesis within the Materials Science Department of the University of Mons, and for her valuable advice, guidance, and support throughout this work.

I would also like to thank my supervisor from Politecnico di Torino, Sara Ferraris, who dedicated her time and support to me despite the distance.

My sincere gratitude also goes to my co-supervisor, Isis Tournay-Dufrenne, for her recommendations, availability, daily help, and constant encouragement.

Also thank to the research center Materia Nova, and especially Lisa Dangreau and Yoann Paint, for their availability, expertise, and the quality of their analyses.

A special thanks goes to all the staff of the Materials Science Department of the Faculté Polytechnique de Mons for their warm welcome, kindness, advice, and support throughout my time in the laboratory.

Thanks to all my friends who, in one way or another, have supported and helped me throughout these years. A special thanks goes to Bob, Fox, and Miri, who, like sisters, shared with me both the joys and the difficulties of university life.

To my sisters, Greta and Federica, thank you for being a constant source of strength and support, especially during the most difficult moments.

To Luca, thank you for always standing by my side with patience, love, and endless support.

To my mom and dad, thank you for always believing in me and supporting all my decisions.

And finally, thanks to my whole family, with a special mention to Uncle Massimo, whom I have always looked up to as an example.

Grazie!

Table of contents

1. Introduction ... 3
   1.1. Theoretical background ... 3
   1.2. Aims and objectives ... 4
   1.3. Structure of the work ... 5
2. Bone tissue and plasma environment ... 5
3. Magnesium and its alloy ... 7
   3.1. Properties ... 7
   3.2. Biocompatibility of alloying elements ... 8
   3.3. Corrosion ... 9
4. Plasma electrolytic oxidation ... 12
   4.1. Generalities ... 12
   4.2. Parameters of the process ... 14
      4.2.1. Electrical parameters ... 14
      4.2.2. Electrolyte composition ... 16
5. Phosphate post-conversion ... 18
6. Drug deposition ... 19
7. Analysis methods ... 21
   7.1. Electrochemical impedance spectroscopy ... 21
   7.2. Scanning electron microscope ... 22
   7.3. X-ray diffraction ... 22
   7.4. Uv-vis spectrophotometry ... 23
8. Materials and methods ... 23
   8.1. Deposition and characterization of the post-conversion phosphate layer ... 23
   8.2. Surface functionalization via bsp drug incorporation ... 25
      8.2.1. Deposition protocol of *depositions a,b,c* and *d*. ... 28
      8.2.2. Deposition protocol of depositions 1 to 10. ... 29
9. Results ... 32
   9.1. Deposition and characterization of the post-conversion phosphate layer ... 32
   9.2. Surface functionalization via bsp drug incorporation ... 45
   9.2.1. First set of deposition - depos a to d ... 45
      9.2.2. Second set of deposition – depos 1 to 10 ... 49
10. Conclusions ... 55
   10.1. Future perspective ... 57

1. INTRODUCTION

1.1. THEORETICAL BACKGROUND

In the case of severe bone fractures, biomedical implants are often required to provide mechanical support throughout the healing process. The implantation of such devices inevitably involves a surgical procedure; therefore, to avoid a second intervention for implant removal after bone recovery, bioresorbable implants are being developed. In this context, biodegradable materials are progressively complementing, and potentially replacing, the traditionally used generations of bio-inert and bioactive materials in orthopaedic applications[1].

Among these, magnesium and its alloys have attracted growing interest due to their intrinsic bioactivity and, above all, their natural biodegradability. Magnesium-based implants can gradually degrade in the physiological environment, potentially eliminating the need for surgical retrieval. Nevertheless, the clinical applicability of these materials requires careful control of their degradation rate in vivo, as well as strict regulation of corrosion processes and the release of any potentially harmful by-products. Even in the absence of toxic degradation products, the prolonged presence of foreign materials in the body may trigger inflammatory responses, sometimes necessitating implant removal. Therefore, beyond simple biodegradability, the biological response to the implant surface plays a crucial role in ensuring long-term clinical success [2].

In addition to their biodegradability, magnesium alloys are particularly attractive because of their favourable mechanical and physical properties. Their Young's modulus and density are comparable to those of natural bone, reducing the risk of stress shielding, a common issue associated with conventional metallic implants. Furthermore, their mechanical strength and fracture toughness make them suitable for load-bearing applications, unlike many polymeric and ceramic biomaterials[1]. Furthermore, magnesium is also interesting for the various designs (screws, plates or other) that can be given to it. Owing to this unique combination of properties, magnesium alloys are considered promising candidates for the development of a new generation of biomedical implants [3].

However, the rapid corrosion of magnesium in physiological environments remains a critical limitation. An optimal implant should degrade in a controlled and progressive manner, maintaining sufficient mechanical integrity during the early stages of bone healing and gradually transferring load to the regenerating tissue. As schematically illustrated in Figure 1.1 a programmed degradation behaviour allows the implant to provide adequate mechanical support during fracture healing, while progressively losing strength as the bone recovers its full mechanical functionality. Achieving such a balance between degradation rate and mechanical stability is essential for the successful clinical translation of magnesium-based implants [1], [4], [5].

Plasma Electrolytic Oxidation (PEO) represents an effective strategy to enhance the corrosion resistance of magnesium alloys, as it enables the formation of a ceramic-like coating strongly bonded to the substrate surface. This layer improves the electrochemical stability of the material while providing surface features, such as controlled roughness and micro and nano scale porosity, that are favourable for bone cell adhesion and tissue integration.

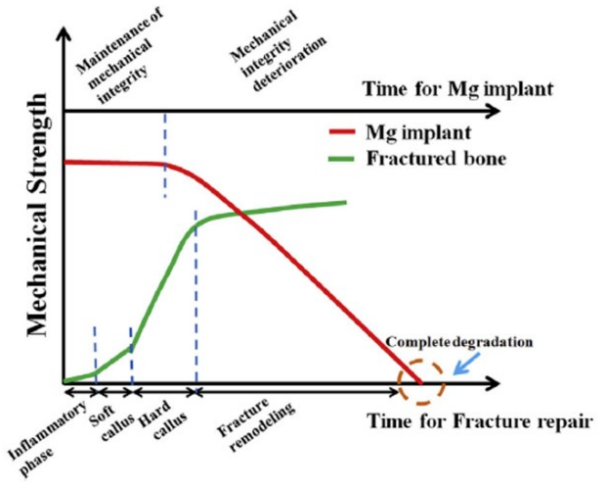


Figure 1.1 - Optimal degradation behaviour of Mg-based implant in bone fracture healing.[4]

1.2. AIMS AND OBJECTIVES

The present research aims to investigate whether the properties of PEO-treated magnesium alloys can be further enhanced through an additional alkaline phosphate conversion treatment. In particular, the study evaluates not only the potential improvement in corrosion resistance but also the capability of the modified surface to promote the adhesion and/or incorporation of the anti-inflammatory Betamethasone Sodium Phosphate (BSP) drug. The incorporation of BSP is expected to modulate the early inflammatory response after implantation, improving the biological acceptance of the device and enhancing overall biocompatibility.

More specifically, the objectives of this work are:

- to characterize the morphology and microstructure of PEO coatings obtained under optimized parameters;
- to assess the effect of the phosphate conversion treatment on corrosion behaviour in physiological-like environments;
- to evaluate the feasibility of drug incorporation within the porous PEO structure;
- to analyse the combined effect of surface modification and drug loading on corrosion resistance, with particular attention to performance in both neutral simulated physiological conditions and inflammation-mimicking environments.

1.3. STRUCTURE OF THE WORK

The first part of this thesis introduces the biomedical context of biodegradable magnesium-based implants, describing bone tissue composition, plasma environment, and the interaction between degrading magnesium and the physiological system.

The properties of magnesium and the selected alloy are presented, with particular attention to mechanical compatibility, corrosion behaviour, and biocompatibility of alloying elements. Furthermore, the corrosion mechanisms of magnesium in physiological environments, and the influence of simulated body fluids are studied.

At a later stage, the Plasma Electrolytic Oxidation (PEO) process is described in detail, covering coating formation mechanisms, microstructural characteristics, and the influence of key process parameters such as electrical parameters, electrolyte composition, and treatment time.

The experimental methodology is then introduced, including materials preparation, surface treatments, electrochemical testing, and characterization techniques. To achieve the objectives of this work, both the experimental section and the discussion of the results are divided into two main parts. The first part focuses on the deposition and analysis of a post-conversion phosphate layer on the PEO coating, with the aim of optimizing the corrosion resistance of the system. The second part investigates a technique for the deposition of the BSP drug, again with the purpose of further enhancing the corrosion resistance of the system.

All results are discussed in terms of corrosion resistance and coating morphology, followed by conclusions and perspectives for future research.

2. BONE TISSUE AND PLASMA ENVIRONMENT

Bones and the skeletal system are integral components of the locomotor system, together with muscles, tendons, and ligaments. They provide structural support and enable movement. Bone tissue is covered by the periosteum, which consists in an outer fibrous layer, an intermediate fibroelastic layer, and an inner osteoblastic layer that is responsible for bone growth and regeneration.

A bone is a complex composite material made up of approximately 10% water, 60% inorganic phase, mainly calcium phosphate responsible for hardness and compressive strength and 30% organic phase, primarily collagen and bone cells, which confer flexibility and resistance to tensile and torsional stresses.

The plasma plays a central role in bone physiology, as it serves as the transport medium for essential ions such as Ca^{2+}, PO_4^{3-}, and Mg^{2+}, as well as for key proteins. It also contributes to the regulation of pH and ionic balance. Bone tissue exists in a dynamic equilibrium with the plasma, characterized by continuous ion exchange between the two compartments. As a result, the bone mineralization is

directly influenced by plasma composition, making plasma the actual physiological environment in which an implant operates in vivo.

During the degradation of magnesium-based implants, the release of Mg^{2+} ions locally modify the concentration of key molecular species involved in bone remodelling, including calcium, phosphate, and signalling molecules. Magnesium is an essential element in bone metabolism, and variations in its extracellular concentration have been shown to directly affect the activity of bone cells. Previous studies have demonstrated that changes in Mg^{2+} levels can modulate osteoblast (that synthesize bone) proliferation, differentiation, and function, while also influencing osteoclast activity (that removes bone tissue). It should be noticed that the biological response to magnesium is strongly dose-dependent: physiological or moderately elevated Mg^{2+} concentrations tend to promote bone formation, whereas excessive levels may disrupt molecular and cellular homeostasis. It should be noticed that the biological response to magnesium is strongly dose-dependent: physiological ($\sim$ 0.8 - 1.0mM) or moderately elevated Mg^{2+} concentrations (2.0 - 4.0 mM) tend to promote bone formation, whereas excessive levels ($>$ 5.0 - 10.0 mM) may disrupt molecular and cellular homeostasis, leading to inhibition of mineralization or cytotoxicity[6], [7]. Therefore, understanding how magnesium is released during corrosion affects both, the local molecular concentrations and the behaviour of osteoblasts and osteoclasts. That is a key aspect in the evaluation and design of biodegradable magnesium-based bone implants [6], [8], [9], [10], [11], [12].

During experimental investigations, corrosive solutions are commonly used to simulate blood plasma and body fluids in order to study the corrosion behaviour of biomedical materials. It is important to consider that no single corrosive medium can perfectly reproduce the physiological environment; therefore, corrosion tests performed in different media may lead to results that are not directly comparable due to the different chemical conditions involved.

Among the most used media, NaCl solution is widely employed in both engineering and biomedical fields. It represents one of the most aggressive corrosive environments, although it poorly reproduces the actual composition of human plasma (which is shown in Table 2.1). As the complexity of the simulated medium increases through the addition of further ionic species, the aggressiveness of the solution generally decreases. One of the main limitations of NaCl solutions is that they do not generate sufficient corrosion products capable of interacting with the system and influencing the subsequent stages of the degradation process.

For this reason, phosphate buffered saline (PBS) is frequently used in biomedical corrosion studies, since it contains salts such as NaCl, KCl, KH_2PO_4 and Na_2HPO_4, making it chemically closer to physiological fluids. The pH of PBS typically ranges between 5.8 and 8. In contact with magnesium substrates, the corrosion products formed in PBS may partially slow down the degradation process

through the formation of magnesium phosphate compounds, while also contributing to the stabilization of the solution pH. Nevertheless, it should be considered that the corrosion rate measured in PBS generally remains higher than that observed under real physiological conditions [11].

Table 2.1 - Inorganic ion concentration in body plasma [8].

Inorganic ions	Na^+	K^+	Ca^{2+}	Mg^{2+}	$(HCO)^{3-}$	Cl^-	HPO_4^{2-}	SO_4^{2-}
Concentration (mmol/l)	142.0	5.0	2.5	1.5	27.0	103.0	1.0	0.5

3. MAGNESIUM AND ITS ALLOY

3.1. PROPERTIES

Magnesium and its alloys have emerged as some of the most attractive engineering metals in recent years. Their growing economic and scientific relevance is reflected in increasingly optimized applications across various industrial sectors. The key feature that distinguishes magnesium is the combination of low density and good mechanical performance [13].

On the other side magnesium exhibits high chemical reactivity, which limits its direct use. The magnesium is prone to rapid corrosion, particularly in aggressive environments or when galvanically coupled with other metals. For this reason, it is almost always used in alloyed form, which improves corrosion resistance and allows broader processability through different forming and metallurgical techniques [13].

What makes magnesium particularly interesting is its lightness, indeed it is the lightest structural metal used in engineering applications, having a density of 1.74 g/cm³, resulting in superior specific mechanical properties compared to aluminium and steel. Table 3.1 lists the main mechanical properties of pure magnesium[13].

Table 3.1- Mechanical properties of pure magnesium[4].

Physical Property	Casted value	Wrought value
Density (g/cm³)	1.74	1.74
Young module (GPa)	41	41
Yield strenght (MPa)	21	100
Compression strenght (MPa)	40	100-140
Tensile strength (MPa)	87	180

Pure magnesium (up to 99.8%) is mainly used in specific chemical and metallurgical applications. In most engineering applications, magnesium alloys are preferred, as they allow better control and modulation of mechanical properties, processability, and corrosion resistance.

When selecting alloying elements, mechanical properties are typically considered first. However, in biomedical research, corrosion resistance and biocompatibility are of primary importance. Therefore, it is essential that the material does not contain elements that may be toxic to the human body.

A typical class of magnesium alloys used in biomedical applications is the Mg–Al–Zn system. In the present research, the AZ31 magnesium alloy was selected, which is composed by Al (2.5-3.5 wt.%), Zn (1.4–1.6 wt.%), Si (<0.3wt.%), Mn (<0.2 wt.%), and balanced Mg [1], [14].

AZ31 exhibits mechanical properties that are close to those of natural bone (Table 3.2), favouring improved biomechanical load transfer and better physiological acceptance of the implant. Moreover, it can be produced through extrusion, rolling, casting, and advanced manufacturing techniques. For biomedical components, casting is the most used processes [3].

Its biocompatibility and biodegradability are adequate for biomedical research purposes. The alloying elements present (Al and Zn) are generally tolerated at low concentrations, although their presence requires a careful evaluation. AZ31 has been extensively studied in both in vitro and in vivo investigations, demonstrating acceptable cellular responses, particularly when protected by appropriate anti-corrosion coatings such as Plasma Electrolytic Oxidation (PEO). Furthermore, as being one of the most commercially available magnesium alloys, AZ31 is widely accessible, cost-effective, and supported by a well-established production chain.

AZ31 is therefore considered a standard material in biomedical research because its composition (Mg–3Al–1Zn) enables reproducible studies, with well-documented mechanical and corrosion behavior and it is widely used as a substrate for testing PEO and other anti-corrosion coatings [2], [3], [15].

Table 3.2- Mechanical properties of different normal tissues compared with available data for currently investigated magnesium alloy (Species, age of species, anatomical location and testing conditions influence the range of values)[3].

Tissue/material	Comp. Strength (MPa)	Tensile strength (MPa)	E-mod. tensile (GPa)	Apparent density (g/cm^3)	Yield strength (MPa)	Elongation (A) at break (%)	Impact strength Charpy V-Notch (J/m^{-2})
Cortical bone	164-240	35-283	5-23	1.8-2.0	--	1.07-2.10	4-70
Cancellous bone	--	1.5-38	10-1570 (MPa)	1.0 – 1.4	--	--	--
AZ31 extruded	83-97	241-260	--	--	165-200	12-16	1.78
AZ31 sheet	110 -180	255-290	--	--	150-220	15-21	1.78

3.2. BIOCOMPATIBILITY OF ALLOYING ELEMENTS

In biomedical engineering, factors such as biocompatibility and rate of degradation are crucial. In fact, the large amount of magnesium and potentially harmful alloying elements released during

corrosion may lead to cytotoxicity, and the degree of toxicity highly depends on the dissolution rate [1] [3].

- Al: the amount of aluminium released from the Mg alloys must be carefully controlled. An Al concentration of 20 ± 7 mmol/l does not induce significant cytotoxicity to several cell lines. Relevant quantities of Al lead to the presence of precipitates on the grain edges, which both increases pitting corrosion and are dangerous for neurons and osteoblasts [3].
- Mn: manganese does not affect the mechanical properties of magnesium alloys significantly but can slightly increase the yield strength. The most important function of Mn is to improve the corrosion resistance by converting iron and other metal elements into relatively harmless intermetallic compounds. A Mn concentration of $1.8 \pm 0.5\,\mu$mol/l induces serious cytotoxicity[3].
- Ca: calcium increases mechanical properties throw both the solid solution strengthening and the precipitate strengthening. Also grain refining and grain boundary strengthening are improved by calcium. Creep resistance is then increased thank to the solid solution strengthening, precipitation strengthening and grain boundary pinning [3].
- Zn: zinc enhances the solid solution strength of magnesium alloy. Furthermore, it improves castability and corrosion resistance. Also the Zn is one of the essential elements of the human body, since it is present in bones and muscular tissues [1].

Both Ca and Zn are essential elements naturally present in the human body and play important roles in numerous physiological processes.

- Rare earth (RE) → RE elements can improve the mechanical characteristics, corrosion properties and creep resistance of Mg alloys. While most of the RE used in the magnesium alloys retard in vivo corrosion, further studies should be carried out in order to evaluate the potential cytotoxicity[3].

3.3. CORROSION

From a biomedical point of view, the degradation rate of magnesium-based implants must be carefully matched to the bone healing process. The implant should maintain sufficient mechanical support during early recovery and gradually transfer load to the regenerating tissue. An excessive rapid degradation can lead to a mechanical failure of the implant, whereas an overly slow corrosion may prolong inflammation and delay the complete tissue restoration [16].

Bone healing and regeneration generally require approximately 12 weeks. Pure magnesium degrades much more rapidly Untreated pure magnesium exhibits an extremely rapid degradation rate in physiological environments, often ranging between 1.0 and 5.0 mm/year, which generally exceeds the ideal clinical threshold required for structural tissue support, that is due to its very negative standard electrode potential (~ –1.7 V_{SHE}) [9], [13] [17].

Moreover, it must be considered that the implant is placed in an already inflamed environment. Its degradation may further increase the inflammatory response, accelerating the degradation process. In addition, proteins and amino acids present in blood plasma interact with inorganic surface components, influencing corrosion mechanisms. The overall complexity of this process is still not fully understood.

The overall corrosion reaction of magnesium in aqueous environments is reported in Equation 1 [3]:

$$Mg_{(s)} + 2H_2O_{(aq)} \rightleftharpoons Mg(OH)_{2\,(s)} + H_{2\,(g)} \quad (1)$$

This global reaction includes the following partial reactions [3]:

$$Mg_{(s)} \rightleftharpoons Mg^{2+}_{(aq)} + 2e^- \text{ (anodic reaction)} \quad (2)$$

$$2H_2O_{(aq)} + 2e^- \rightleftharpoons H_{2\,(g)} + 2OH^-_{(aq)} \text{ (cathodic reaction)} \quad (3)$$

$$Mg^{2+} + 2OH^- \rightleftharpoons Mg(OH)_{2\,(s)} \text{ (precipitation reaction)} \quad (4)$$

The magnesium hydroxide formed during corrosion deposits on the substrate surface, providing partial protection against further attack by water; however, when the chloride ion concentration exceeds approximately 30 mmol/L, the protective film progressively deteriorates. Considering that physiological fluids contain about 104 mmol/l Cl^-, magnesium hydroxide progressively converts into highly soluble magnesium chloride [3].

The conversion of $Mg(OH)_2$ into $MgCl_2$ makes the implant surface significantly more reactive and susceptible to corrosion. The formation of chloride can be expressed as:

$$Mg^{2+} + 2Cl^- \rightarrow MgCl_2 \quad (5)$$

$$Mg(OH)_2 + 2Cl^- \rightarrow MgCl_2 + 2OH^-_{(aq)} \quad (6)$$

This behaviour is strongly influenced by the markedly different solubility of the two compounds: $Mg(OH)_2$ is only sparingly soluble in water (solubility product at 25°C: $K_{sp}(Mg(OH)_2=5.61x10^{-12})$, thus forming a partially protective surface layer, whereas $MgCl_2$ is highly soluble and readily dissolves into the surrounding electrolyte, preventing the formation of a stable barrier [18], [19].

During the development of the bone cell–surface bonding, the initial condition of the surface plays a crucial role. Corrosion of Mg-based implants generates four main components:

- a corroded surface layer,
- dissolved magnesium ions (and alloying elements),
- hydroxide ions (OH^-),
- hydrogen gas.

Hydrogen evolution may lead to the formation of gas pockets, potentially causing tissue necrosis and/or delayed healing. A clearer understanding of the pH influence on magnesium stability can be obtained using the Pourbaix diagram (Figure 3.1).

In magnesium alloys such as AZ31, corrosion behaviour is further influenced by microstructural heterogeneities. The presence of secondary phases (e.g., β-$Mg_{17}Al_{12}$) may generate microgalvanic coupling between the α-Mg matrix and intermetallic particles. These local galvanic cells accelerate anodic dissolution of the magnesium matrix and promote localized degradation phenomena, increasing the overall corrosion rate.

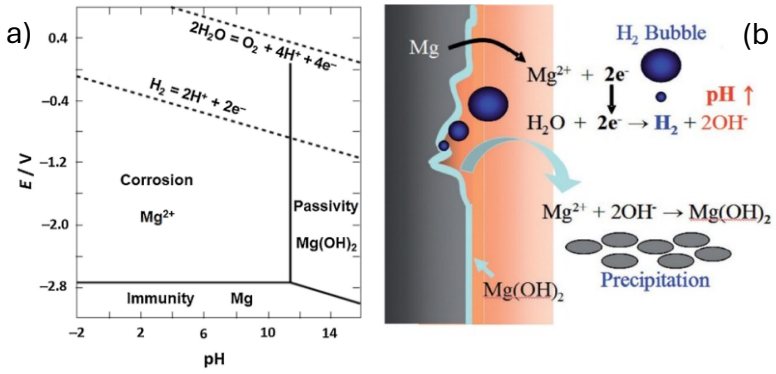


Figure 3.1 - (a) Pourbaix diagram of Mg; (b) schematic representation of magnesium corrosion in aqueous environments showing H_2 bubble formation [1].

To investigate corrosion behaviour under physiological conditions, simulated body fluids are commonly employed. These in vitro solutions typically contain buffering agents such as HCO_3^-, HPO_4^{2-} or Tris-HCl, which neutralize the OH^- ions generated during magnesium dissolution and mitigate abrupt pH increases at the metal/solution interface. However, direct correlation between in vitro and in vivo results remains challenging, as the biological environment is far more complex and dynamically regulated; consequently, in vitro tests frequently report faster degradation rates.

In the present research, phosphate-buffered saline (PBS) was used as the testing medium. In PBS, the main corrosion products of magnesium are magnesium hydroxide and magnesium phosphates, while insoluble carbonates may also form due to dissolved CO_2. The coexistence of PO_4^{3-} and CO_3^{2-} ions promotes the precipitation of sparingly soluble compounds on the metal surface. This precipitation results in the formation of a partially protective layer that can temporarily reduce the corrosion rate even in chloride-containing environments, as phosphate and carbonate species complex Mg^{2+} ions and limit their diffusion into the bulk solution [9], [11], [20].

Nevertheless, compared to standard laboratory solutions such as PBS or Simulated Body Fluid (SBF), blood plasma represents a more physiologically relevant environment due to the presence of proteins. Immediately after implantation, plasma proteins adsorb onto the metallic surface, forming a so-called protein corona. This adsorbed layer can either reduce uniform corrosion by acting as a diffusion barrier or promote localized attack by inducing differential aeration or complexation effects. Furthermore, proteins can bind Mg^{2+}, Ca^{2+} and PO_4^{3-} ions, thereby modifying local ionic equilibria, influencing the solubility of corrosion products, and affecting the nucleation and growth of phosphate or carbonate phases [9], [11], [20].

4. PLASMA ELECTROLYTIC OXIDATION

4.1. GENERALITIES

The Plasma Electrolytic Oxidation (PEO) process is a surface-coating technique derived from conventional anodization, enabling the formation of ceramic-like coatings on light metal alloys such as magnesium alloys. The formation of electrical micro-arcs, typical of this anodic process, induces plasma, electrochemical, and thermo-chemical reactions, which contribute to the growth of a highly adherent oxide layer on the metallic substrate. The resulting coating is extremely hard and wear-resistant, furthermore it improves the corrosion resistance of the underlying metal. Moreover, the PEO coating exhibits a characteristic surface roughness and micro and nano scale porosity, which are essential for promoting cell adhesion and tissue growth[15].

The magnesium alloy is the anode of the electrochemical cell of the PEO process, while a stainless-steel cathode is used. The electrolyte is typically a weakly alkaline or a slightly acidic, making PEO an environmentally friendly approach compared with other coating technologies. For biomedical application an alkaline electrolyte is used.

The process generates high surface temperatures and intense sparking phenomena that locally melt the metal, which then reacts with oxygen species present in the electrolyte. Figure 4.1 illustrates the mechanism of coating growth and the formation of pores and cracks [15].

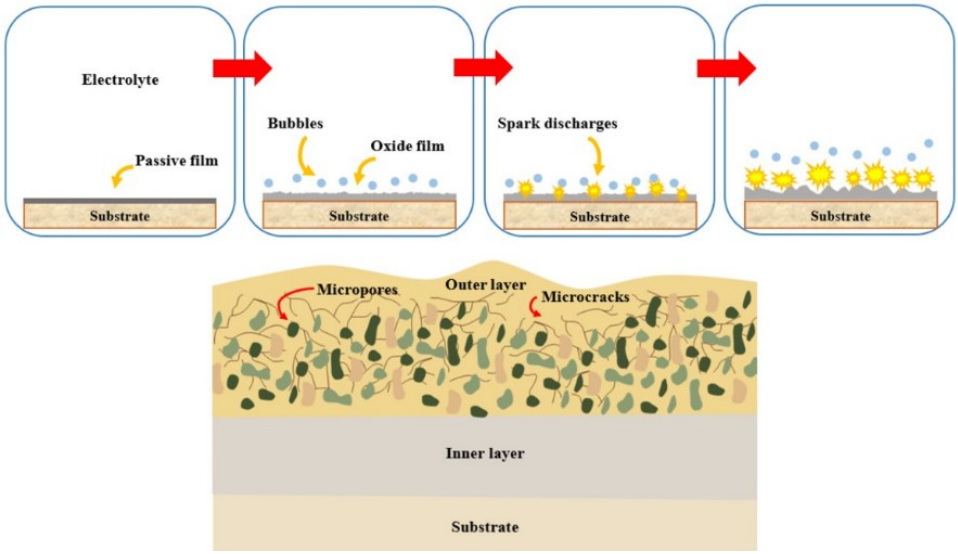


Figure 4.1-The growth mechanism of the coating and the formation of pores and cracks in the PEO process[1].

During the Plasma Electrolytic Oxidation process, schematically shown in Figure 4.2, the coating forms through a sequence of electro, thermal and plasma induced reactions that progressively modify the metal surface. In the initial stage, the application of an anodic potential leads to a rapid increase in voltage until the breakdown limit of the native oxide layer is reached. At this point, the first micro-discharges appear, localized in regions where the electric field is strongest. These discharges propagate within discharge channels characterized by extremely high current densities and electric

field intensities, which raise the local temperature up to thousands Kelvin. Under these extreme conditions, plasma-chemical reactions occur simultaneously with localized metal melting and vaporization, gas bubble formation, and oxide deposition on the channel walls.

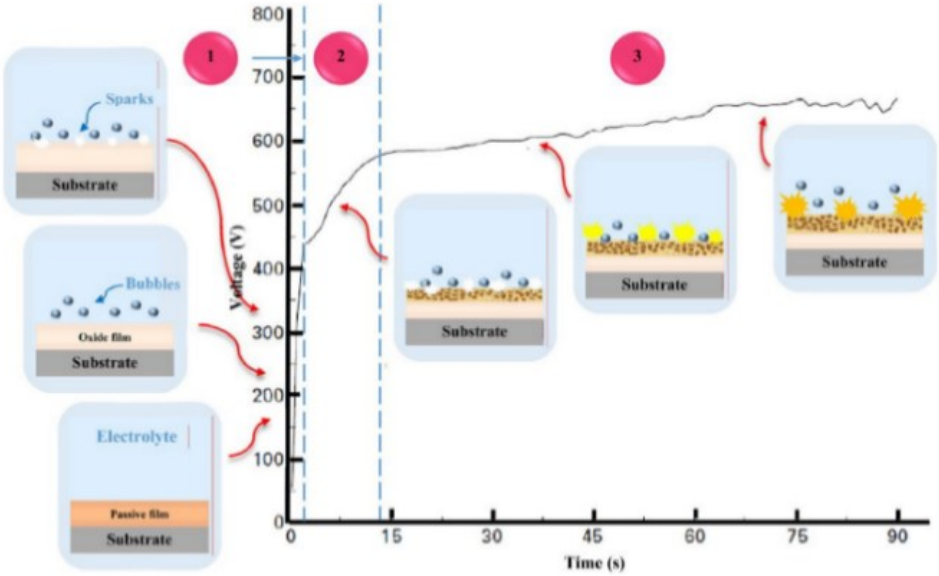


Figure 4.2-Schematic of the cell potential-time and formation process of PEO coating [1].

Figure 4.3 shows how discharge intensity and distribution evolve over time. In the very first seconds (0–3 s), only a few weak and discrete bright spots are visible, corresponding to isolated micro-discharges. As the process progresses (15–30 s), the discharges grow in size and intensity while decreases in number; this reflects the increasing energy associated with each discharge and the transition to a more stable micro-arc regime [15].

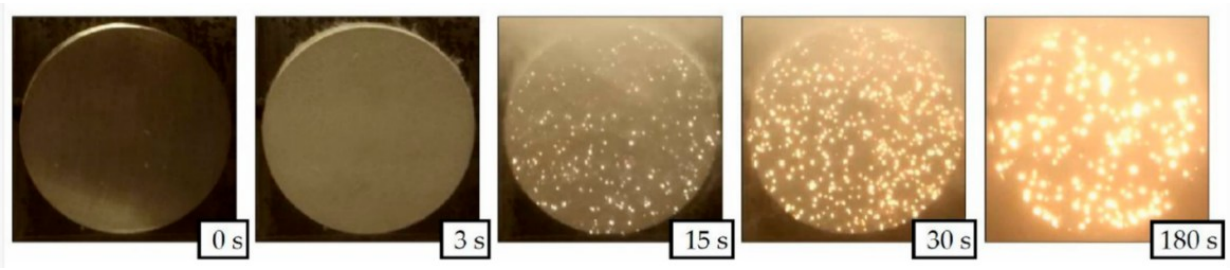


Figure 4.3- Evolution of discharge distribution and intensity in relation to the process time for the PEO of an AZ31 magnesium alloy in alkaline silicate electrolyte. Brightness correlates with discharge intensity on the respective surface region of the sample [15].

These phenomena lead to the development of the characteristic multilayer structure of PEO coatings, illustrated in Figure 4.4. At the interface with the substrate, a nanometers-thick barrier layer forms, which is compact, nearly defect-free, and crucial for coating adhesion and barrier performance, called *thin inner dense layer*. Above this, a thicker and relatively dense working layer develops, produced by repeated melting-solidification cycles and oxide accumulation under the applied electric field. The outermost layer, known as the *porous outer layer*, is highly porous due to gas entrapment and the rapid cooling of molten regions during discharge events. The increasing porosity of this technological

layer makes it the most susceptible to corrosion, whereas the internal barrier layer plays the primary role in protecting the substrate [1], [15], [21].

If the process parameters are not properly optimized, excessively large discharges may occur, damaging the coating or causing local delamination. For this reason, precise control of process conditions is essential to avoid detrimental discharge events and to ensure stable growth of the oxide layer [1], [15], [21].

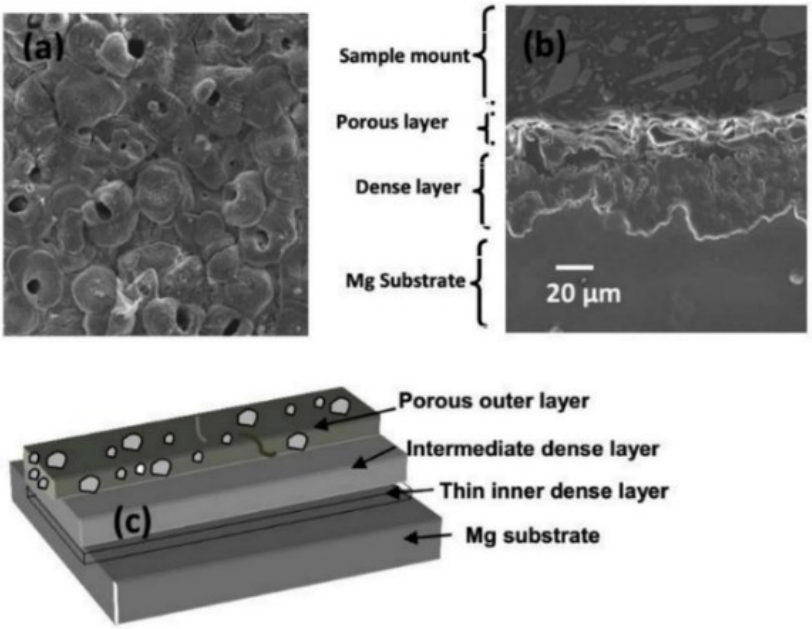


Figure 4.4- Schematic of a PEO treated sample, (a) surface, (b) structure, and (c) layer in PEO coating [1].

4.2. PARAMETERS OF THE PROCESS

The PEO process requires to carefully monitor and tune several parameters in order to control the final properties of the resulting material. It is possible to divide the process parameters into two groups: the electrical parameters and the electrolytic solution parameters. All parameters affect each other, so the whole system should be considered during the final study. within the system. By controlling these parameters, it is possible to regulate the thickness and morphology of the resulting film [1], [15], [22].

4.2.1. ELECTRICAL PARAMETERS

Electrical parameters include current density, final voltage, frequency, and duty cycle. These parameters affect the transfer process of anions, which move mainly by diffusion, convection, or electrical migration during the coating process; therefore, they directly influence the electric field[1].

4.2.1.1. VOLTAGE

Voltage influences the formation of the outer layer, which becomes thicker as the voltage increases. However, excessive thickening leads to excessive pore growth, which negatively affects corrosion resistance properties [1].

4.2.1.2. CURRENT DENSITY

Current density represents the driving force of the process. If it is too high, the process becomes excessively aggressive: highly energetic sparks generate larger pores and cracks, ultimately impairing the corrosion resistance of the coating.

Although current density strongly affects coating growth and morphology, several studies suggest that, compared to other electrical parameters, its direct influence on corrosion resistance and biocompatibility may be less significant [1], [15].

4.2.1.3. ELECTRICAL REGIME

The control of process parameters in Plasma Electrolytic Oxidation (PEO) is strongly influenced by the selected electrical regime. Under continuous current or voltage (DC) conditions, micro-plasma discharges remain intense and persistent throughout the treatment, potentially causing irreversible damage to the growing film and, in severe cases, to the substrate. To mitigate these effects and achieve a more controlled oxide growth, pulsed or alternating/bipolar regimes are commonly adopted.

In a unipolar pulsed regime, the current is alternatively switched ON and OFF phases. The interruption of current flow promotes system relaxation, redistribution of ionic species, and stabilization of electrochemical gradients. Although the OFF time may allow some chemical dissolution, it often enhances barrier layer formation while limiting the duration and intensity of discharge events[15].

In bipolar regimes, a cathodic phase is added to the anodic one responsible for oxide growth. The cathodic component can partially reduce the oxide and modify the active interfacial zone. Although cathodic discharges are generally less energetic, they may locally heat the coating and lower the breakdown threshold during the subsequent anodic phase.

After barrier layer formation, the system acts as a capacitor, and current can flow only above a threshold voltage (Ut) associated with oxide breakdown. An increase in Ut over time typically indicates coating thickening and reduced defect density.

Overall, pulsed and especially bipolar regimes improve energy control, reduce destructive discharges, and promote the formation of a more compact and corrosion-resistant coating [15].

4.2.1.4. FREQUENCY

Frequency is another fundamental parameter in the PEO process and corresponds to the number of pulses per second. High frequencies help reduce micro-cracks and control surface roughness, leading to smoother coatings with finer microstructures and, consequently, improved corrosion resistance.

At lower frequencies, each pulse delivers higher energy, promoting faster film growth. The discharges become more intense and energetic, causing greater material melting and oxide formation. However, the resulting coating typically exhibits higher surface roughness [1].

4.2.1.5. DUTY CYCLE

The duty cycle represents the ratio between the ON time and the total cycle time (ON + OFF) and is therefore directly related to the average energy supplied to the system during the PEO process. A high duty cycle implies a longer current application time per cycle, resulting in greater energy input and increased surface temperature. This promotes faster coating growth and greater thickness but may also lead to increased pore size and surface roughness due to more intense and prolonged discharges. Conversely, a lower duty cycle reduces the energy introduced per cycle, limits discharge duration, and allows longer cooling periods between pulses, favouring the formation of a more compact coating with lower defect density. Therefore, optimization of the duty cycle is crucial to balance thickness, porosity, and corrosion resistance of the coating [1].

4.2.2. ELECTROLYTE COMPOSITION

The electrolyte composition plays a fundamental role in coating formation. The chemistry of the electrolyte influences the nature and size of the pores, as well as the phases present in the coating. Depending on the electrolyte composition, the voltage and processing time parameters must also be adjusted, as the coating growth rate varies accordingly.

Selecting the appropriate electrolyte solution is essential to obtain a coating suitable for biodegradable biomedical implants. In particular, the electrolyte must be free of toxic elements to ensure biocompatibility [1], [15].

4.2.2.1. POTASSIUM HYDROXIDE SOLUTION

Magnesium oxide cannot form in an acidic environment, whereas in an alkaline environment it forms a partially protective film, the potassium hydroxide so is used [1].

4.2.2.2. SODIUM SILICATE-BASED SOLUTION (Na_2SiO_3)

The addition of Na_2SiO_3 to a KOH solution promotes the formation of a denser and more uniform film at the anode. The presence of SiO_3^{2-} ions is beneficial for developing coatings with enhanced corrosion resistance. Although adding Na_2SiO_3 increases the coating growth rate, an excessive silicon concentration may lead to the formation of an overly porous layer; therefore, the Si content must be carefully optimized [1].

In scientific literature, phosphate-based compounds (e.g., PO_4^{3-}) are often employed for similar purposes[1]. However, preliminary experiments conducted in the early stages of this research showed that coatings produced using Na_2SiO_3 exhibited superior quality and improved corrosion resistance compared to those obtained with phosphate additives. Moreover, several studies have reported that silicon is incorporated more effectively into PEO coatings than PO_4^{3-} species [14], [16].

4.2.2.3. FLUORIDE BASED SOLUTION

Fluoride contributes significantly to the formation of the PEO ceramic film due to its high electronegativity, which allows it to react immediately with Mg^{2+} ions. This interaction triggers a growth mechanism during plasma discharges: due to their high electrolytic affinity, fluoride ions F^- react preferentially with the substrate compared to hydroxyl ions OH^-. This process leads to the formation of a highly stable magnesium fluoride MgF_2 phase, according to the following reaction (Equation 7):

$$Mg^{2+} + 2F^- \rightarrow MgF_2(s) \quad (7)$$

The resulting layer, primarily concentrated within the inner barrier layer, is remarkably compact and dense. Sparks and high local temperatures reached during the process accelerate MgF_2 precipitation over less stable oxides. Fluoride acts as a critical sealing agent for the micro-pores and discharge channels typically generated during the PEO process. Since MgF_2 has extremely low solubility, it provides a superior physical barrier that prevents the excessive dissolution of the magnesium substrate into the physiological solution. Its stability not only prevents tissue necrosis but actively promotes osteoblast adhesion and proliferation, ensuring that F^- ion release remains well within the safety limits for the implant's biocompatibility. Specifically, while low fluoride concentrations (between 10 and 50 μM) actively stimulate osteoblast proliferation and differentiation, levels exceeding 100 μM are known to induce cytotoxicity and impair bone mineralization [23].

Several studies have compared different fluoride compounds to determine the most suitable additives for biomedical applications. While LiF was found to form films with ideal morphological uniformity, compounds such as NaF and Na_2SiF_6 exhibited higher corrosion resistance and lower hydrogen release. For these reasons, NaF was selected for the experimental procedure of this research, as it ensures an optimal balance between coating density, electrochemical stability, and biological acceptance [1], [14], [24].

4.2.2.4. GLYCEROL

Glycerol is a dense chemical compound that modifies the viscosity of the electrolyte solution. Its primary role is to alter the micro-discharges during the PEO process, reducing their intensity and thereby promoting the formation of a more homogeneous, dense, and less porous coating [16].

The increased viscosity and the reduced conductivity of the solution result in slower and more controlled film growth. This leads to fewer deep pores, which prevents excessive penetration of harmful ions (e.g., chlorides) and enhances the electrochemical stability of the coating.

Glycerol also influences the incorporation of other elements from the electrolyte bath, promoting a more uniform distribution of silicon and phosphorus. These elements contribute to the formation of a compact and stable ceramic phase [16].

5. PHOSPHATE POST-CONVERSION

Following the PEO process, a phosphate post-conversion treatment was carried out. This surface treatment was performed for two main reasons: to reduce the surface porosity and consequently improve the corrosion resistance of the coating, and to functionalize the surface to enhance its interaction with Betamethasone Sodium Phosphate (BSP) [21].

Phosphate conversion coatings are based on the interaction between the substrate and the treatment bath, leading to the physical deposition of a phosphate layer chemically bonded to the surface. During immersion, magnesium locally dissolves, releasing Mg^{2+} ions, while the reduction of H^{+} ions causes a local increase in pH, promoting the precipitation of magnesium phosphate compounds directly onto the substrate surface [25].

These treatments are of particular interest in the biomedical field because they improve the biocompatibility of magnesium-based systems. However, obtaining uniform phosphate layers remains challenging, since coatings are often fragile and poorly adherent. For this reason, in the present work the phosphate conversion treatment was applied onto a previously formed PEO layer, exploiting the porous oxide structure to promote both mechanical and chemical anchoring of the phosphate coating.

The most widely studied phosphate conversion treatments are calcium phosphate (Ca–P) systems, since calcium and phosphorus are the main inorganic constituents of human bone. Their presence on implant surfaces promotes faster interaction with bone tissue and supports healing processes.

The deposition conditions of the phosphate conversion bath play a critical role in determining the quality and biological performance of the resulting layer. Temperature, pH, and immersion time are the main process parameters. Increasing the bath temperature generally promotes nucleation and leads to denser and more uniform coatings; however, excessively high temperatures may induce intense hydrogen evolution, causing porosity and cracks. Similarly, the pH controls both substrate dissolution and phosphate precipitation kinetics: excessively acidic conditions may damage the underlying PEO layer, whereas excessively alkaline conditions may inhibit the Mg^{2+} release required for phosphate nucleation. Immersion time also strongly affects the coating morphology, since excessively prolonged treatments may result in partial dissolution or detachment of the already formed layer.

Although Ca–P treatments are the most commonly reported in the literature, sodium-phosphate-based systems have also been investigated for magnesium alloys because they should provide improved control of the deposition process and favour the formation of thinner and more uniform phosphate layers on PEO-treated surfaces, contributing to pore sealing and corrosion protection [21], [25], [26].

In the present study, phosphate conversion was performed on AZ31 magnesium alloy substrates previously treated by PEO, in order to further modify the surface chemistry and improve the

biological functionality of the system. The treatment was carried out by immersion in an alkaline phosphate solution prepared from phosphoric acid (0.5 M) and sodium hydroxide (3 M), at pH 9 and 60°C, under continuous stirring to promote uniform deposition. These conditions were selected because they also allowed preservation of the underlying PEO layer. Within the broader research project in which this study is included, different temperatures and pH values had previously been investigated, and pH 9 at 60°C was identified as the optimal condition for phosphate deposition without compromising the integrity of the PEO coating. Three immersion times (30 minutes, 1 hour, and 2 hours) were investigated to evaluate their influence on the morphology, thickness, and protective properties of the phosphate layer formed on the AZ31+PEO system.

6. DRUG DEPOSITION

As previously mentioned, when an implant is inserted in vivo, it may trigger an inflammatory response from the body[27]. The inflamed environment is rich in superoxide ($O_2^{\bullet -}$) and hydrogen peroxide (H_2O_2), which are produced as part of the immune response against bacteria and foreign bodies. These Reactive Oxygen Species (ROS) significantly influence the corrosion behaviour of magnesium. During inflammation, the local pH around the implant can decrease from the physiological value of 7.4 to approximately 5.5, and it may take up to 15 days to return to normal conditions [28].

Referring to the Pourbaix diagram of magnesium (see Figure 3.1), $Mg(OH)_2$ forms a stable layer only under alkaline conditions (pH ≥ 10.4). In neutral or acidic environments, this layer loses stability, leading to an increase in corrosion kinetics. Furthermore, aggressive chloride ions (Cl^-) can penetrate through the micro-pores and micro-cracks of the PEO coating, attacking the inner dense layer and eventually reaching the metallic substrate [29].

The incorporation of an anti-inflammatory drug into the porous PEO layer offers a dual benefit. First, it partially fills and seals the pores, reducing surface roughness and porosity (as reported in Table 6.1), thereby limiting the penetration of chloride ions. Second, the controlled release of the drug helps to reduce the inflammatory response in the surrounding tissue. In this way, corrosion resistance is improved both physically (by barrier enhancement) and biologically (by inflammation control). A schematic representation of this improvement mechanism is shown in Figure 6.1.

Corticosteroids are among the most widely used drugs for controlling inflammatory responses. Betamethasone Sodium Phosphate (BSP) belongs to this class, its chemical structure is shown in Figure 6.2 [28].

Table 6.1- The average values with standard deviations of relative surface porosity, thickness and roughness of the PEO and PEO/BSP coating [28].

Coating type	Relative surface porosity (%)	Thickness (µm)	Roughness(µm)
PEO	56.7 ± 1.8	18.7 ± 2.3	1.45 ± 0.31
PEO/BSP	18.3 ±0.7	23.9±1.5	0.86 ± 0.11

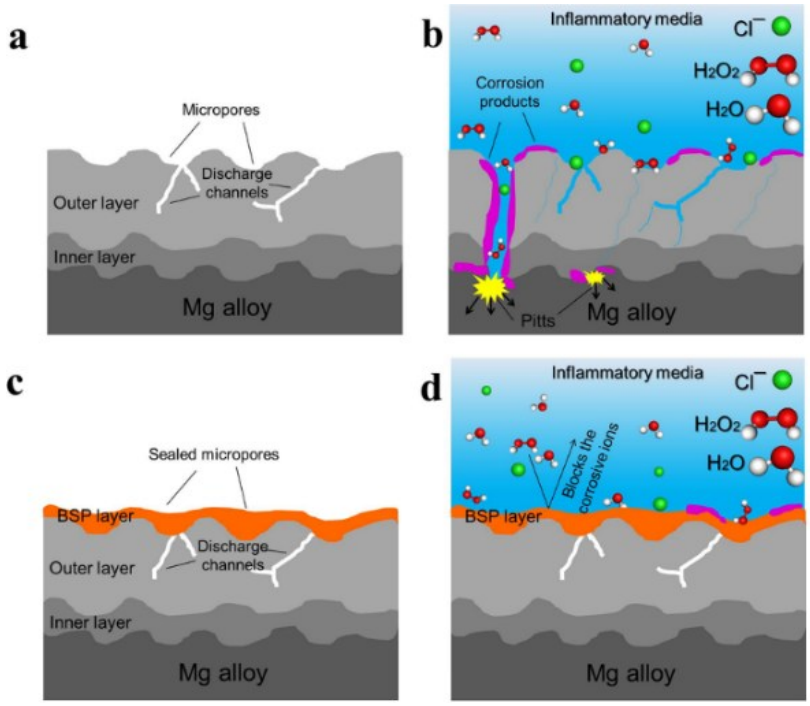
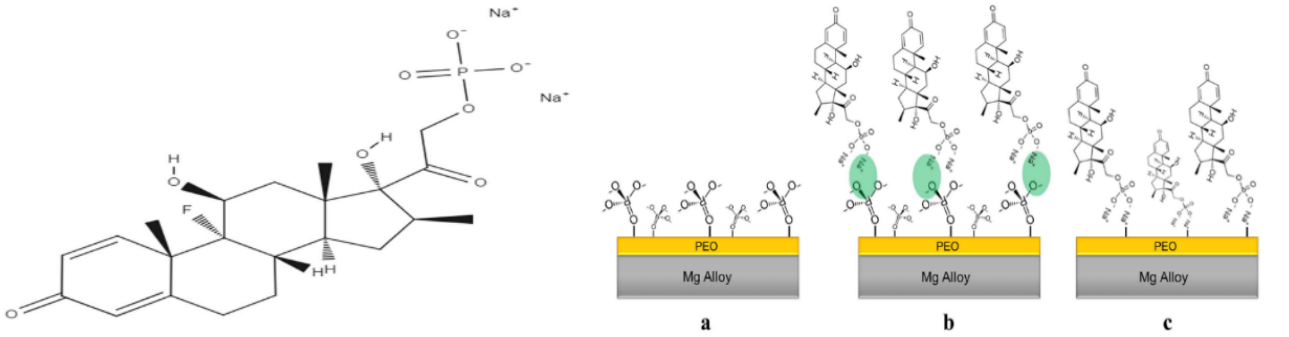


Figure 6.1- Schematic representation of the corrosion mechanism of the (a,b) PEO and (c,d) PEO/BSP coating inflammatory condition [28].

To maximize the drug incorporation and its subsequent controlled release, it is essential to ensure high compatibility between the PEO layer and BSP. For this reason, surface functionalization of the ceramic coating is required to enhance its chemical affinity with the drug [30].

Since BSP is composed of phosphate (PO_4^{3-}) and sodium (Na^+) ions, improving the interaction between these ionic species and the PEO coating can promote stronger bonding and more efficient incorporation. The mechanism is schematically reported in Figure 6.2. In some cases, such ions are already present in the coating due to their addition to the electrolyte during the PEO process. However, in the present study, phosphates were not introduced directly into the electrolyte bath. Instead, alternative drug incorporation strategies were employed, as described in detail in chapter 8.



a) b)

Figure 6.2 - (a) Chemical structure of the betamethasone sodium phosphate drug, (b) schematic representation of the preparation of PEO/BSP coating[28].

7. ANALYSIS METHODS

In the following paragraph the aim is of presenting the analysis techniques used and the reason why they have been chosen for the research.

7.1. ELECTROCHEMICAL IMPEDANCE SPECTROSCOPY

Electrochemical Impedance Spectroscopy (EIS) is one of the most effective techniques for studying corrosion behaviour, thanks to its non-destructive nature, high reproducibility, and sensitivity to even very small corrosion rates. In an EIS measurement, the system's response is expressed as a complex impedance composed of a real part (Z′) and an imaginary part (Z″). The real component represents the resistive contributions of the system, including the solution resistance, the charge-transfer resistance at the metal/electrolyte interface, and the resistance associated with protective layers such as PEO coatings. The imaginary component instead reflects the capacitive and inductive behaviour of the interface: capacitive effects, dominant in magnesium systems, arise from the dielectric properties of surface films and the electrical double layer, while inductive features at low frequencies are typically associated with relaxation phenomena such as adsorption or metastable pitting.

EIS measurements are typically carried out using a three-electrode electrochemical cell, consisting of a working electrode (the sample under investigation), a reference electrode with a stable potential, and a counter electrode that completes the circuit. The measurements are usually performed in an aggressive electrolyte (PBS in this research) to simulate corrosive service conditions.

EIS is performed by applying a small sinusoidal voltage perturbation and measuring the resulting current over a wide frequency range. This frequency-resolved approach allows the separation of fast electrochemical processes, such as double-layer charging, from slower mechanisms related to the growth, dissolution, or transformation of corrosion products. The resulting impedance spectra are commonly represented in Nyquist and Bode plots, which enable the identification of the electrochemical behaviour of the surface and the extraction of parameters such as charge-transfer

resistance and polarization resistance, both directly related to the corrosion rate of magnesium. Because of its high sensitivity to subtle changes in the system, EIS is particularly valuable for assessing protective coatings like PEO layers, allowing the distinction between the compact inner layer and the porous outer layer and enabling the monitoring of their evolution during immersion [13].

7.2. SCANNING ELECTRON MICROSCOPE

The Scanning Electron Microscope (SEM) creates magnified images of morphology, topography, and chemical composition for the sample. In the SEM, an electron beam is focused on the sample in vacuum condition. The interaction between the sample and the material generate different kind of signal, which are collected to recreate the image. The image is generated point by point converting the emitted signal:

- the secondary electrons emitted give information about the superficial topography;
- the back scattered electrons (EBS) of higher energy are used to analyse the chemical composition.

Many SEMs can analyse X-rays emitted by the interaction of the sample with the primary electrons. This technique allow the chemical analysis reproducing elemental distribution maps, used for qualitative analysis [31].

7.3. X-RAY DIFFRACTION

In this work, X-ray Diffraction (XRD) is used to determine how the immersion in the phosphate solution and the presence of Betamethasone Sodium Phosphate (BSP) works and whether it produces measurable changes in the surface phases of the PEO-treated magnesium alloy. XRD is a non-destructive technique that identifies crystalline compounds by analysing the diffraction peaks generated by the interaction between the X-rays and the atomic planes of the material. After the treatment, the appearance of new peaks or the modification of existing ones allows to understand if PBS-derived phosphates or corrosion products, such as magnesium phosphates or $Mg(OH)_2$, have formed on the surface. The same approach is applied here to evaluate whether BSP molecules, which contain phosphate groups, may participate in the formation of new crystalline or semi-crystalline phases when interacting with the PEO layer. Although BSP may remain partly amorphous, making its direct detection more difficult, XRD can still reveal indirect signatures of its incorporation, such as the formation or growth of phosphate-rich phases. Reference patterns for magnesium-phosphate compounds help to verify these changes and confirm if the drug contributes to the modified surface chemistry. By comparing diffraction patterns before and after exposure to BSP, the technique helps

to clarify whether the drug has been retained, incorporated, or has influenced the formation of phosphate-containing reaction layers on the magnesium surface [32].

7.4. UV-VIS SPECTROPHOTOMETRY

Ultraviolet-Visible spectrophotometry (UV-Vis) is an absorption spectrometry technique which involves part of the UV electromagnetic spectrum and the full visible one.

The sample is immersed into a corrosive solution during the studied period, then part of it is extracted to be analysed. The solution is placed into a cuvette inside the spectrophotometer chamber. A beam of light from passes through the sample, and the instrument measures the amount of UV-Vis radiation absorbed by the sample. The cuvettes are usually made of materials transparent to these wavelengths. Using the Beer-Lambert law, reported in the Equation 8, it is possible to calculate the concentration of the absorbing species in the solution.

$$A = \varepsilon l C \tag{8}$$

Where A is the absorbance, ε is a constant, l is the path length and C the concentration of the absorbing substance.

In this work, UV-Vis spectroscopy is used to measure the concentration of BSP in the solution over time. More specifically, the release of the drug BSP is investigated by monitoring its absorbance and, consequently, its concentration in the corrosive solution [33].

8. MATERIALS AND METHODS

To address the research question, the following experimental approach was adopted: the experimental procedure consisted of a multi-step surface preparation and characterization route designed to ensure reproducible coating formation and reliable analysis. The process was divided into two main stages. The first focused on the deposition and characterization of a post-conversion phosphate layer on the PEO coating, with the aim of optimizing its corrosion resistance. The second stage investigated a method for depositing the BSP drug, again with the goal of enhancing the overall corrosion resistance of the system and to add anti-inflammatory properties to the surface.

8.1. DEPOSITION AND CHARACTERIZATION OF THE POST-CONVERSION PHOSPHATE LAYER

The first step consists in preparing the sample for the PEO treatment. The sample is a AZ31 magnesium alloy sheet with a size of 60 mm × 50 mm × 5 mm (provided by KG Fridman AB, Karlstadt, Sweden) with the following mass fraction: Al 2.5-3.5%, Zn 0.7-1.3%, %Mn 0.2%, Ni 0.1%, Si 0.05%, Cu 0.05%, Ca 0.04%, Fe 0.0005% and the rest is Mg. Firstly, it was subjected to a chemical etching pretreatment to remove native oxides and surface contaminants. This step involved sequential

immersion in nitric acid (HNO_3), first at 2 M and then at 0.25 M, with intermediate rinsing in deionized water to eliminate residual reagents and prevent cross-contamination [34].

Subsequently, the PEO treatment was performed. The electrolyte solution (2 L total volume) was prepared using distilled water with the addition of potassium hydroxide (KOH, 8.41 g/L), sodium silicate ($Na_2SiO_3 \cdot 5H_2O$, 10.49 g/2 L), sodium fluoride (NaF, 1.93 g/L), and glycerol (50 mL/L). The process was carried out under continuous stirring and controlled thermal conditions using an external cooling system. The PEO process was performed using a PowerPulse-Micronics system, applying a bipolar waveform consisting of an anodic pulse at 400 V for 5 ms, followed by a cathodic pulse at −30 V for 5 ms, with an off-time (Toff) of 5 ms. The operating frequency and duty cycle were 67 Hz and 66.7%, respectively.

In the following step, a phosphate conversion treatment was carried out to further modify the surface. This involved the preparation of a phosphoric acid solution (0.5 M) and a sodium hydroxide solution (3 M). Within the broader research project in which this study is embedded, it was demonstrated that optimal phosphate deposition, without damaging the underlying PEO layer, is achieved at pH 9, with a treatment duration of 1 hour at a temperature of 60 °C. Throughout the process, continuous stirring was maintained in order to promote the formation of a uniform phosphate-based layer.

Once the sample is prepared the corrosion resistance and the characterisation of the coating layers are studied, doing a comparison between the three different times of phosphate post-conversion.

The corrosion resistance was investigated by electrochemical impedance spectroscopy (EIS) using a BioLogic SP-300 potentiostat. Measurements were performed in a three-electrode electrochemical cell housed inside a Faraday cage to minimize external noise. The sample acted as the working electrode, a platinum electrode as the counter electrode, and an Ag/AgCl (3 M KCl) electrode as the reference. A circular area of 1 cm^2 of the sample surface was exposed to the electrolyte. The electrolyte used was phosphate-buffered saline (PBS), composed of 8 g/L NaCl, 0.2 g/L KCl, 1.2 g/L Na_2HPO_4, and 0.2 g/L KH_2PO_4, with a buffered pH of 7.43. Prior to EIS measurements, the open circuit potential (OCP) was monitored for 15 minutes to ensure system stabilization. EIS spectra were then acquired using a sinusoidal perturbation of 10 mV rms over a frequency range from 100 kHz to 100 mHz, after 2 h, 6 h, and 24 h of immersion.

The typical behaviour of a PEO coating analysed by Electrochemical Impedance Spectroscopy (EIS) reflects the characteristic structure of the coating, generally composed of an outer porous layer and the barrier layer. In the interpretation of EIS results, this structure is usually manifested by the presence of two time constants, observable in Bode plots. At high frequencies, the contribution of the outer porous layer is observed, while at medium-low frequencies the response of the inner barrier layer appears, which is mainly responsible for the corrosion resistance of the coating.

The equivalent circuit used to describe the electrochemical behaviour of a PEO coating consists of an electrolyte resistance R_s, followed by two RC branches or, more frequently, constant phase elements (CPEs) associated with the two coating layers. In this model, $R_p$represents the resistance of the porous layer, generally lower and less protective, $R_b$represents the resistance of the barrier layer, which is considered the most important parameter for evaluating the corrosion protection efficiency of the treatment. The use of CPEs instead of ideal capacitors is related to the surface inhomogeneity of the coating and to the presence of porosity, roughness, and local current distribution effects.

In Bode plots, a well-formed PEO coating typically exhibits high impedance modulus values at low frequencies, indicating good corrosion resistance. Furthermore, the presence of two distinct phase angle maxima is generally associated with the two functional layers of the coating. As the coating degrades or the immersion time increases, a decrease in the low-frequency impedance modulus and a reduction or merging of the time constants are often observed, indicating the progressive loss of effectiveness of the barrier layer and the gradual activation of the magnesium substrate.

Surface morphology and chemical composition were analysed using scanning electron microscopy (SEM) coupled with energy-dispersive spectroscopy (EDS) (Hitachi SU8020, Hitachi, Tokyo, Japan). For microstructural analysis, the specimens were mounted in resin and subjected to a standard metallographic preparation procedure, including sequential grinding and polishing with progressively finer abrasives. Final cleaning was performed using ethanol and compressed air to obtain a smooth, defect-free surface suitable for high-resolution SEM observation[35].

X-ray diffraction (XRD) analysis was carried out using a Malvern Panalytical Empyrean diffractometer in grazing incidence mode (ω = 1°) to minimize the contribution of the substrate to the diffraction patterns. Measurements were performed using a copper anode (λ = 1.54 Å), with a step size of 0.01° and a counting time of 3 seconds per step. Grazing incidence XRD was employed to investigate the crystalline structure of the coating.

All characterization and corrosion studies were also carried out on a bare AZ31 sample and on a sample subjected only to PEO treatment, without phosphate post-conversion.

8.2. SURFACE FUNCTIONALIZATION VIA BSP DRUG INCORPORATION

The second phase of this research focused on identifying a suitable method for depositing Betamethasone Sodium Phosphate onto PEO-coated AZ31 magnesium alloy specimens. The primary objective was to evaluate the feasibility of drug incorporation within the surface coating system and to assess whether the presence of BSP could further modulate the corrosion behaviour of the material in a physiologically relevant environment. Betamethasone Sodium Phosphate (BSP), sourced from the pharmaceutical product Celestone® Soluspan® (Merck & Co., Inc.), was used as the drug for

deposition. This phase was conducted following the results obtained in the first stage of the project (Section 4.1), which established the optimal conditions for the phosphate conversion treatment.

A total of thirteen deposition conditions were investigated, systematically varying the phosphating parameters (pH, temperature, and duration), the surface pre-treatment steps (PBS rinsing, ethanol immersion), and the drug deposition strategy. Initially, four samples (A, B, C, and D) were prepared and analyzed (see Section 8.2.1). The results of these analyses prompted a revision of the analytical method. So, ten additional samples (Depos 1 to 10) were produced and are described in Sections 8.2.2 and 8.2.3. All the drug solution preparations and solution depositions were applied by dip-coating. The sample was maintained under constant stirring using a magnetic stirrer, ensuring adequate homogenization while excessive agitation.

The deposition of Betamethasone Sodium Phosphate is carried out by dissolving the drug in the solvent at a ratio of 3 mg per 1 mL of solvent. The drug used is commercially available and is stored in solid form in a refrigerator to ensure proper preservation[28].

Once the solution is prepared (200 mL), the sample is vertically immersed in the beaker and kept in the solution for 1 hour. Subsequently, the sample is placed in a drying chamber under low-humidity conditions (set to 0% humidity, with the instrument's minimum achievable level being approximately 20%) at a temperature of 30 °C.

The characterization of the drug deposition was initially investigated using SEM and EDS, under the same operating conditions described in Section 8.1. Later, the effective deposition of the drug was evaluated with a double-beam UV–Vis spectrophotometer (PerkinElmer Lambda 365), for which 2 cm^2 of the sample surface were exposed to 60 mL of the analytical medium. The analysis process is reported in Figure 8.1. the measurements were performed after 2h, 6h, 24h, and from 2 to 7 days at a wavelength of $\lambda = 242$ nm, corresponding to the characteristic absorption peak of BSP, over a spectral range from 220 nm to 300 nm [22].

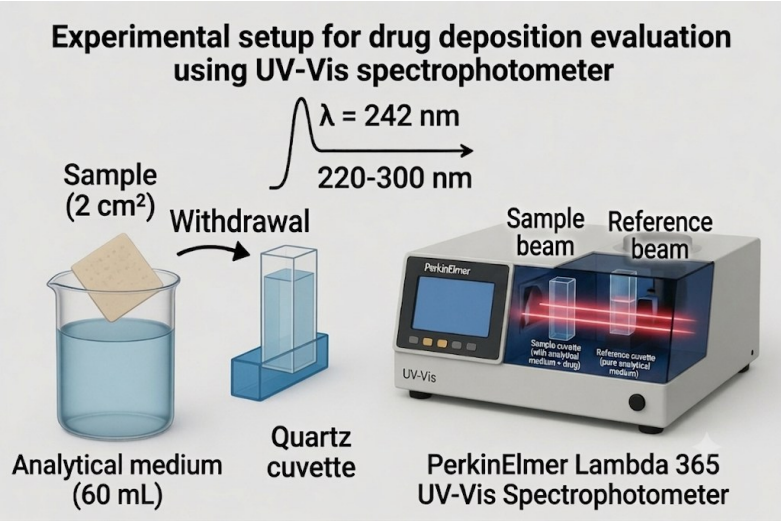


Figure 8.1- Schema of the UV-VIS spectrophotometry analysis process.

To determine the concentration of drug released from the material, the calibration curves were constructed for both 0.1M NaCl and PBS solutions by preparing samples with progressively increasing concentrations of PBS. The concentration range started from 1.00×10^{-6} mol L^{-1} and was increased up to the maximum level detectable by the instrument (Table 8.1). The calibration curve obtained in NaCl is shown in Figure 8.2, while the calibration curve for PBS is presented in Figure 8.3.

Table 8.1 – Absorbance of BSP in NaCl and PBS in function of the concentration.

Concentration (mol L^{-1})	Absorbance in NaCl	Absorbance in PBS
$1.00 \cdot 10^{-06}$	0.08	0.13
$5.00 \cdot 10^{-06}$	0.07	0.17
$1.00 \cdot 10^{-05}$	0.17	0.21
$5.00 \cdot 10^{-05}$	0.70	0.64
$1.00 \cdot 10^{-04}$	1.42	Out of range
$5.00 \cdot 10^{-04}$	Out of range	Out of range

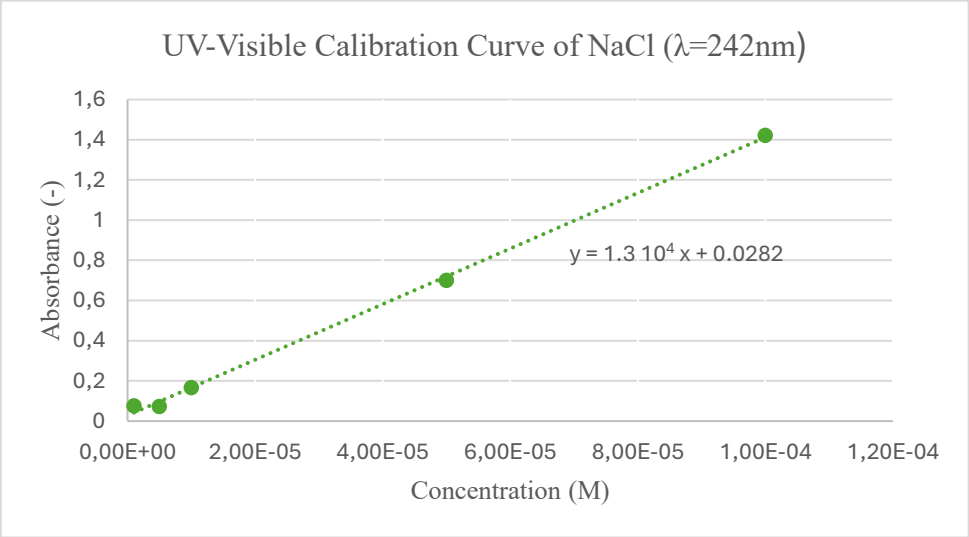


Figure 8.2- UV-Visible Calibration Curve of NaCl.

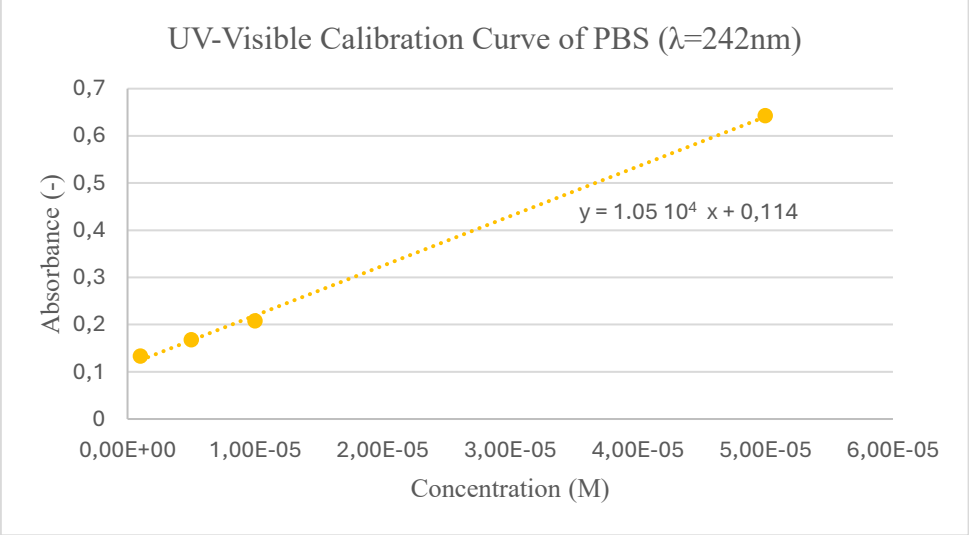


Figure 8.3 - UV-Visible Calibration Curve of PBS.

8.2.1. DEPOSITION PROTOCOL OF *DEPOSITIONS A,B,C* AND *D*.

According to the considerations discussed previously, samples A to D were analysed using the two solvents recommended in the pharmaceutical datasheet of the drug[36]. Samples Depos A and Depos B were prepared using methanol-based BSP solutions, whereas samples Depos C and Depos D employed distilled water as the deposition medium. In Table 8.2. Samples A, B, C, and D were processed according to the following procedures:

- Depos A (*Ph1h_methAx3*): PEO treatment followed by 1 h of phosphate post-conversion. The drug deposition was then carried out via vertical immersion in 200 mL of a methanol + BSP solution, followed by 1 h of drying in a dedicated chamber. The immersion and drying steps were repeated for a total of three times.
- Depos B (*Ph2h_methBx3*): PEO treatment followed by 2 h of phosphate post-conversion. The drug deposition was performed via vertical immersion in 200 mL of a methanol + BSP solution, followed by 1 h of drying in a dedicated chamber. The immersion and drying steps were repeated three times in total.
- Depos C (*Ph1h_h2oCx3*): PEO treatment followed by 1 h of phosphate post-conversion. The drug deposition was carried out via vertical immersion in 200 mL of a distilled water + BSP solution, followed by 1 h of drying in a dedicated chamber. The immersion and drying steps were repeated three times in total.
- Depos D (*Ph2h_h2oDx3*): PEO treatment followed by 2 h of phosphate post-conversion. The drug deposition was performed via vertical immersion in 200 mL of a distilled water + BSP solution, followed by 1 h of drying in a dedicated chamber. The immersion and drying steps were repeated three times in total.

The choice to use distilled water and methanol as solvents was made based on the information provided in the drug's leaflet, which indicates its solubility in both media.[37]

This set of samples was analysed by UV–Vis spectroscopy using 0.1 M NaCl as the analytical medium.

Table 8.2 - Protocol deposition for samples Depos A to D.

SAMPLE	PHOSPHATING CONDITIONS	PBS RINSE	DRUG DEPOSITION METHOD	ETHANOL STEP 30% EtOH	MEDIUM ANALYSIS
Depos A: *Ph1h_methAx3*	T=60°C, pH 9, t=1h	No	BSP/methanol: 3x wetting cycle 1h, dessicator 1h	No	NaCl
Depos B: *Ph2h_methBx3*	T=60°C, pH 9, t=2h	No	BSP/methanol: 3x wetting cycle 1h, dessicator 1h	No	NaCl
Depos C: *Ph1h_h2oCx3*	T=60°C, pH 9, t=1h	No	BSP/methanol: 3x wetting cycle 1h, dessicator 1h	No	NaCl
Depos D: *Ph2h_h2oDx3*	T=60°C, pH 9, t=2h	No	BSP/methanol: 3x wetting cycle 1h, dessicator 1h	No	NaCl

8.2.2. DEPOSITION PROTOCOL OF DEPOSITIONS 1 TO 10.

The experimental conditions investigated in the second set of samples (Depos 1 to 10) were designed to systematically explore the effect of three independent variables on BSP incorporation: (i) the surface pre-treatment steps (PBS rinsing and ethanol immersion), (ii) the drug deposition method (aqueous bath, methanol cycles, and aqueous cycles), and (iii) the phosphating protocol applied prior to drug loading, considering that the reference temperature is 60 °C; therefore, samples treated under these conditions are not explicitly labelled in the specimen nomenclature. The detailed processing protocols are summarized in Table 8.3.

Initially, a new set of samples (Depos 8 and Depos 9) was produced using the same deposition strategy previously adopted for Depos A–D but limiting the procedure to a single wetting–drying cycle. This approach was introduced to evaluate whether partial dissolution of the deposited BSP could occur during subsequent deposition cycles. In particular, Depos 8 was prepared using a methanol-based BSP solution, while Depos 9 employed a distilled water-based solution.

Subsequently, an immersion step in ten-times diluted PBS was introduced for selected samples (Depos 1, 3, 4, 6, and 10). This treatment was expected to improve the properties of the freshly deposited coating layer, since PBS contains phosphates, NaCl, and physiologically relevant ionic species. In particular, the rehydration promoted by PBS may favour rearrangement of the surface phosphate groups and increase surface wettability, thereby enhancing BSP adhesion and deposition homogeneity while also reducing localized corrosion phenomena. Moreover, PBS acts as a buffer solution, contributing to surface pH stabilization and promoting more favourable conditions for subsequent drug deposition [9], [11].

A brief immersion (1–2 s) in a 30% ethanol solution after BSP deposition was also introduced in selected samples to promote partial precipitation and retention of the drug within the porous PEO structure. Since Betamethasone sodium phosphate exhibits limited solubility in ethanol while being highly soluble in water and methanol [38], the ethanol-assisted step was expected to mainly enhance solvent evaporation and reduce possible redissolution phenomena. Owing to its high volatility and lower surface tension, ethanol can also facilitate penetration of the solution inside the pores of the coating, improving BSP retention, homogeneity, and stability [39], [40].

In Depos 1, after the PBS immersion step, BSP deposition was carried out by vertical immersion for 1 h in an aqueous solution buffered at pH 7 using 0.01 M NaOH and 0.01 M H_3PO_4. During the deposition process, the pH was continuously monitored in order to avoid fluctuations that could alter the stability and effectiveness of the active pharmaceutical ingredient. After deposition, the sample was briefly immersed in diluted ethanol and finally dried in a desiccator for 1 h.

In Depos 2, drug deposition was experimentally performed simultaneously with the phosphate post-conversion treatment. For this purpose, the phosphating bath was prepared using phosphoric acid (0.5

M) and sodium hydroxide (3 M), adjusting the pH to 8 before dissolving BSP. The treatment was then carried out for 1 h at 40 °C. These modified conditions were selected to preserve the stability of the drug, which is known to be sensitive to high temperatures and strongly acidic or alkaline pH values, while still maintaining conditions as close as possible to those investigated in Section 8.1 [30]. The same phosphating conditions were subsequently applied for 1 h (Depos 3) and 2 h (Depos 4), followed by the conventional BSP deposition step, to evaluate the influence of treatment duration on subsequent drug incorporation.

The absence of the expected phosphate and drug contents in the previous analyses (Section 9.2.2) suggested that phosphorus species could already be incorporated into the porous PEO structure directly from the electrolyte. Therefore, in Depos 5, K_3PO_4 was introduced into the PEO electrolyte in place of sodium silicate, maintaining the same concentration. BSP deposition was then directly carried out using the aqueous immersion method.

Based on the results obtained in Section 9.2.1, deposition using methanol-based solutions was further investigated through an additional pipette-assisted drop coating approach consisting of five consecutive wetting–evaporation cycles (Depos 6).

Finally, Depos 7 was designed to evaluate the possibility of forming a phosphate layer beneath the PEO coating. The objective was to create a phosphate-rich anchoring layer located at the base of the PEO porosities, potentially improving BSP retention during the subsequent deposition step. The entire set of samples was subsequently analysed by UV–Vis spectroscopy using PBS as the analytical medium.

Table 8.3 - Summary of experimental conditions for BSP drug deposition on PEO-coated AZ31 magnesium alloy.

SAMPLE	PHOSPHATING CONDITIONS	PBS RINSE	DRUG DEPOSITION METHOD	ETHANOL STEP 30% EtOH	MEDIUM ANALYSIS
Depos 1: *1_Ph91h_acq_PBS_eth*	T=60°C, pH 9, t=1h	Yes t=90s	Aqueous bath pH 7 ($NaOH/H_3PO_4$ 0.01M), 1h; desiccator 1h	Immersion 1sec	PBS
Depos 2 *2_ph8T40_BSPinPhosp*	T=40°C, pH 8, t=1h	No	Drug deposition during the phosphate conversion.	No	PBS
Depos 3 3_*ph8T401h_acqu_BSP_eth*	T=40°C, pH 8, t=1h	Yes t=90s	Aqueous bath pH 7 ($NaOH/H_3PO_4$ 0.01M), 1h; desiccator 1h	Immersion 1sec	PBS
Depos 4 *4_ph8T402h_acqu_BSP_eth*	T=40°C, pH 8, t=2h	Yes t=90s	Aqueous bath pH 7 ($NaOH/H_3PO_4$ 0.01M), 1h; desiccator 1h	Immersion 1sec	PBS
Depos 5 *5_ K_3PO_4PEO_acqu_BSP_eth*	PEO with K_3PO_4 in the electrolyte, + phosphate conversion at T=60°C, pH 9, t=1h	No	Aqueous bath pH 7 ($NaOH/H_3PO_4$ 0.01M), 1h; desiccator 1h	Immersion 1sec	PBS
Depos 6 *6_Ph91h_meth_PBS_drop*	T=60°C, pH 9, t=1h	Yes t=90s	BSP/methanol: 5 wetting–drying cycles	No	PBS
Depos 7 *7_Ph5_PBS_acqu_BSP*	Bare Mg: pH 5, T=60°C, t=1h; then PEO	No	Aqueous bath (H_2O + BSP, pH adjusted), 1h; desiccator 1h	No	PBS
Depos 8 *8_Ph91h_PBS_meth_BSPx1*	T=60°C, pH 9, t=1h	No	BSP/methanol: single wetting cycle 1h, dessicator 1h	No	PBS
Depos 9 *9_Ph91h_PBS_h2o_BSPx1*	T=60°C, pH 9, t=1h	No	BSP/H_2O: 1 wetting–drying cycles	No	PBS
Depos 10 *10_Ph91h_PBS_acqu_BSPx1*	T=60°C, pH 9, t=1h	Yes t=90s	Aqueous bath pH 7 ($NaOH/H_3PO_4$ 0.01M), 1h; desiccator 1h	No	PBS

9. RESULTS

9.1. DEPOSITION AND CHARACTERIZATION OF THE POST-CONVERSION PHOSPHATE LAYER

SEM-EDS Characterisation

The surface morphology and chemical composition of the samples have been investigated before and after 24 hours of immersion in PBS.

In order to provide a baseline for understand and compare the effects introduced by the surface treatments, an exam of the pure alloy behaviour has been useful. The AZ31 substrate initially exhibited a smooth surface with minimal morphological features (Figure 9.1) and was primarily composed of Mg (79.9 wt%), with minor contributions from Al (4.6 wt%) and Zn (2.2 wt%), consistent with the nominal composition of the alloy under investigation, as reported in Table 9.1.

After 24 hours of immersion, the surface has been subjected to a pronounced morphological transformation, characterized by the formation of needle-like crystalline corrosion products and an amorphous phase. The EDS results, reported in Table 9.1, showed a significant increase in oxygen content, from 11.6 to 42.4 wt%, the appearance of phosphorus (at 20.1 wt%) and potassium (at 9.7 wt%), and a decrease in magnesium content. These changes are consistent with the formation of corrosion products generated during immersion in PBS. The literature shows that is not easy to identify a specific deposition compound formed after the immersion in PBS. The predominantly semicrystalline and amorphous nature of the corrosion layer prevents precise phase identification. Nevertheless, the presence of magnesium phosphates, magnesium hydroxide, and carbonates is commonly reported, and confirmed by experimental results, with the latter often attributed to the dissolution of CO_2 into the solution*[9]*.

It is interesting to note how the same alloy can exhibit different corrosion behaviours, as shown in Figure 9.2. This occurs because the alloy may contain precipitates and locally different microstructural features, each one can lead to a different corrosion response. This is yet another reason why a surface treatment, like the PEO, can provide greater reliability and predictability for a biomedical implant.

Table 9.1- EDS composition of bare AZ31 before and after 24h of immersion in PBS.

(weight%)	C	O	Na	Mg	P	K	Al	Zn
AZ31 0h	1.8	11.6	79.9	79.9	--	--	4.6	2.2
AZ31 24h	1.2	42.4	7.0	19.0	20.1	9.7	0.6	--

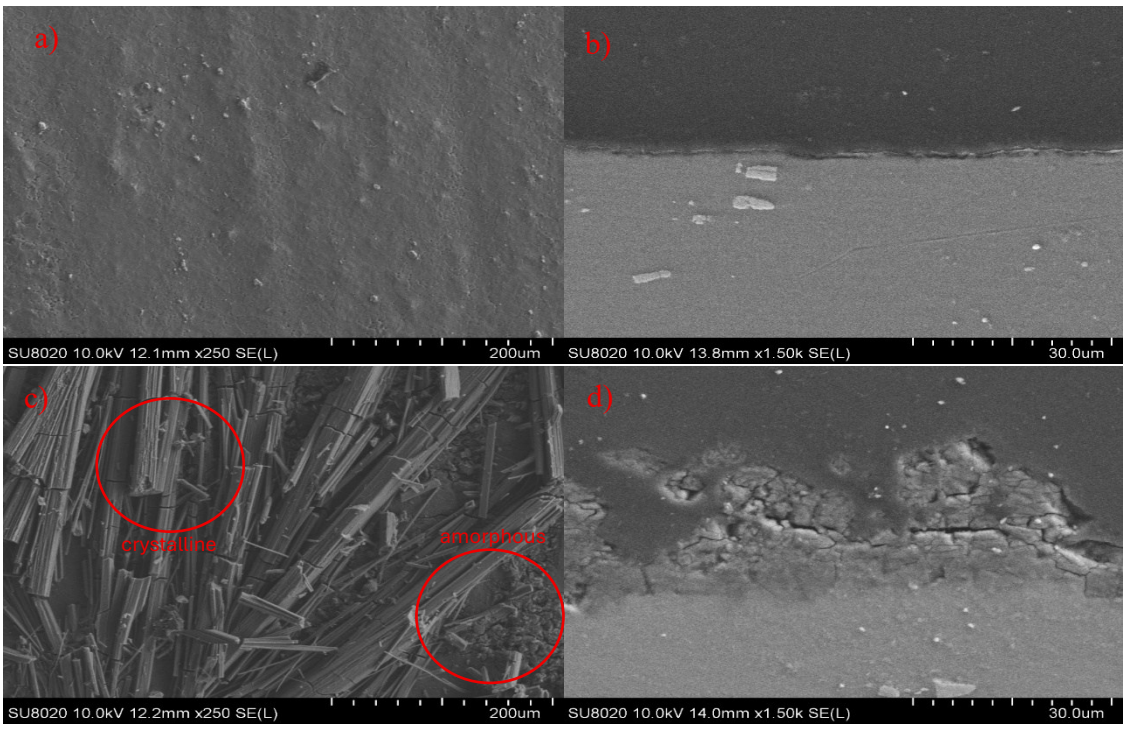


Figure 9.1 - Bare AZ31 SEM images: a) surface after 0h of immersion in PBS, b) cross-section 0h of immersion in PBS, c) surface 24h of immersion in PBS, d) cross-section 24h of immersion in PBS.



Figure 9.2 - Bare AZ31 corroded after 24h of exposition to PBS.

The PEO layer, without the phosphate post conversion treatment, exhibited the characteristic porous morphology typical of plasma electrolytic oxidation coatings as shown in Figure 9.4 (a), with an outer porous layer and an inner denser region, as confirmed by cross-sectional observations in Figure 9.4 (b). The layer thickness, measured by the SEM cross-sections, ranged approximately from 8 to 12.5 µm. At the macroscopic scale, the sample assumes an opaque appearance, associated with the increase in surface porosity and roughness., as shown in Figure 9.3. The EDS analysis, which results are reported Table 9.2, confirmed a composition rich in Mg 40wt%, O 41.5wt%, and Si 14.3wt%, reflecting the incorporation of silicate species from the electrolyte during the PEO process. After 24 hours of PBS immersion, the surface of the PEO layer was also covered by needle-shaped corrosion products, and the chemical composition shifted notably, with the appearance of N 6.2wt% and P

22.2wt%, and the disappearance of Si, suggesting a partial dissolution of the outer porous layer and deposition of phosphate-based compounds from the PBS solution.

Table 9.2 - EDS results of PEO, PEO + 30 min, 1h, 2h phosphate post-conversion treatement samples, before and after 24h of immersion in PBS.

	PEO		Phosphate post-conversion 30 min		Phosphate post conversion 1h		Phosphate post-conversion 2h	
exposition	0h	24h	0h	24h	0h	24h	0h	24h
C (%wt)	1.3	0.8	0.7	1.1	0.8	1.2	1.2	1.1
O (%wt)	41.5	41.2	46.6	40.5	47.6	41.1	45.7	41.1
Na (%wt)	--	6.5	14.5	7.4	23.0	6.0	10.2	6.6
Mg (%wt)	40.0	15.1	16.4	14.7	13.5	15.4	17.0	15.3
Al (%wt)	1.3	--	1.0	0.1	0.7	--	1.8	0.4
Si (%wt)	14.3	0.6	5.4	0.8	3.8	0.5	7.2	1.1
P (%wt)	--	21.5	15.4	22.6	18.4	23.9	15.1	21.1
Ca (%wt)	--	--	--	--	1.5	--	1.7	--
K (%wt)	0.9	14.3	--	12.8	--	11.7	--	13.1
F (%wt)	0.7	--	--	--	--	--	--	--

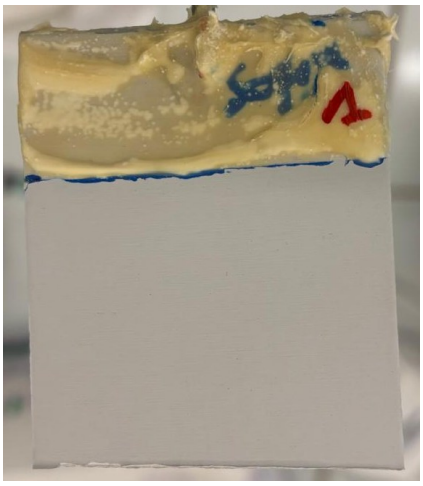


Figure 9.3 - Surface of a sample after the PEO process.

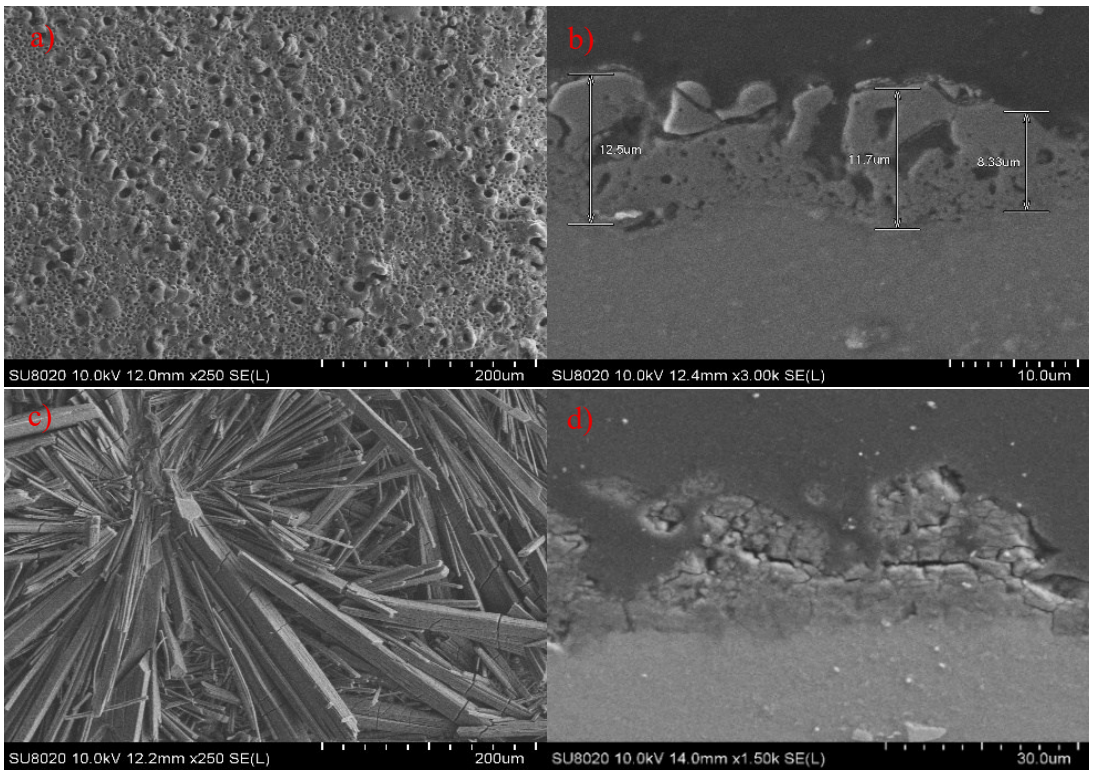


Figure 9.4 – PEO layer SEM images: a) surface after 0h of immersion in PBS, b) cross-section 0h of immersion in PBS, c) surface 24h of immersion in PBS, d) cross-section 24h of immersion in PBS.

The specimens treated with the phosphate post-conversion process were then analysed. The immersion time in the solution was different for everyone, specifically 30 minutes, 1 hour, and 2 hours. A first comparison between the phosphate post-conversion specimens and those treated only with PEO showed that the porosity present in the PEO layer is filled by the post-conversion treatment. In fact, as seen in the cross-section in

Figure 9.5, an additional layer clearly forms on top of the PEO coating, and material is deposited inside the pores. A comparison of the surfaces as well, shown in Figure 9.6, confirms that the deposition of the phosphate post-conversion layer fills the porosities, leading to a more homogeneous surface, an aspect of great importance for corrosion resistance, as it prevents corrosive agents from penetrating into the pores. Results confirmed also by the mapping of elements reported in Table 9.4.

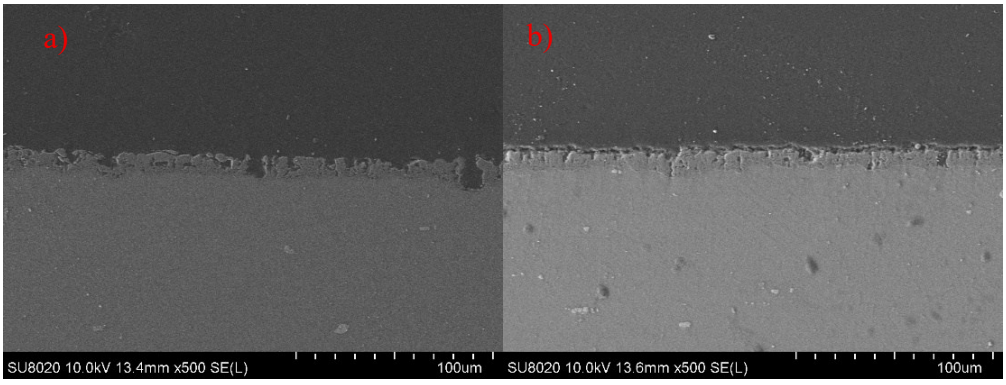


Figure 9.5 - Cross-section SEM images of (a) PEO coating, (b) PEO coating + 1h phosphate post-conversion.

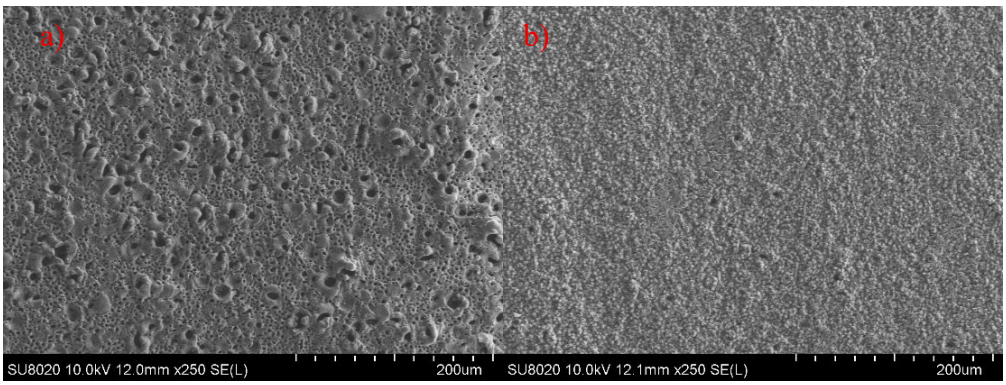


Figure 9.6 - Surface SEM images of (a) PEO coating, (b) PEO coating + 1h phosphate post-conversion.

By comparing the cross-sections obtained for the different treatment times, shown in Figure 9.7, a deposited layer can be observed on the top of the coating in all three specimens. In the case of the 30-minute treatment (a), this layer is less pronounced than in the other two. However, when examining the image at higher magnification (Figure 9.8), it becomes clear that a thinner, yet still present, layer has formed, which also fills the porosities.

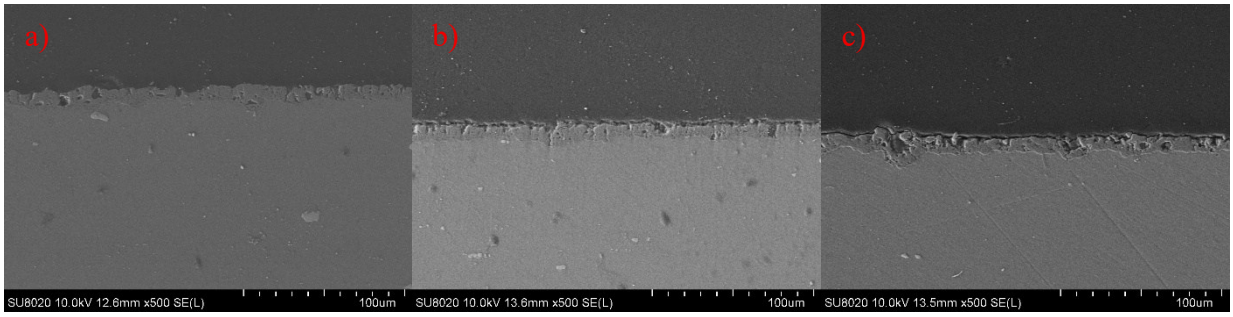


Figure 9.7 - Cross-section SEM images: a) 30 min phosphate conversion- 0h immersion in PBS, b) 1h phosphate conversion - 0h immersion in PBS, c) 2h phosphate conversion - 0h immersion in PBS.

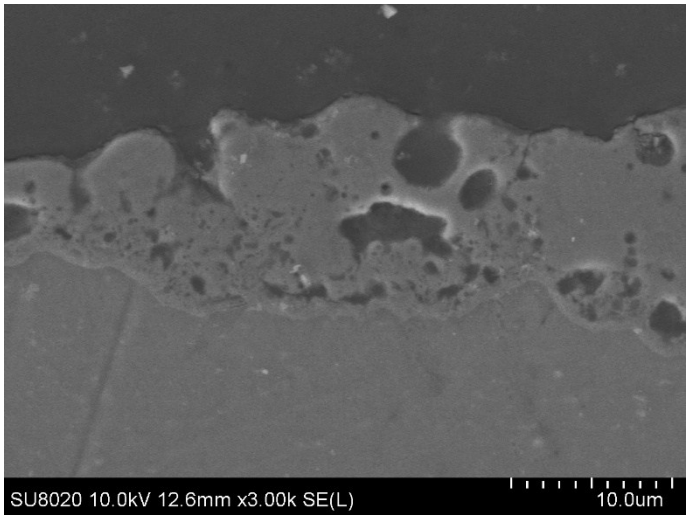


Figure 9.8 - Cross-section of PEO + 30min phosphate post-conversion sample with magnification 10 um.

An additional feature observed exclusively in the specimen treated for 30 minutes is highlighted in Figure 9.9 that reveals the presence of two distinct regions at the top surface of the sample: one characterized by open porosity and another where the pores appear sealed by the layer deposited

during the treatment. Moreover, according to the EDS results (Table 9.3), it seems that a 30 minutes treatment is not sufficient to achieve a continuous coating, which may also explain the lower corrosion resistance measured by EIS, compared (see later) to the samples treated for 1h and 2h. In fact, the amount of P detected in the porous region is 6.6 wt%, whereas in the filled area it reaches 10.2 wt%. The same trend is observed for Na, which increases from 6.9 wt% to 12.6 wt%. It is interesting to note, as shown in Figure 9.10, that this behavior does not occur in the 1-hour and 2-hour specimens, where the analysis revealed a much higher degree of uniformity.

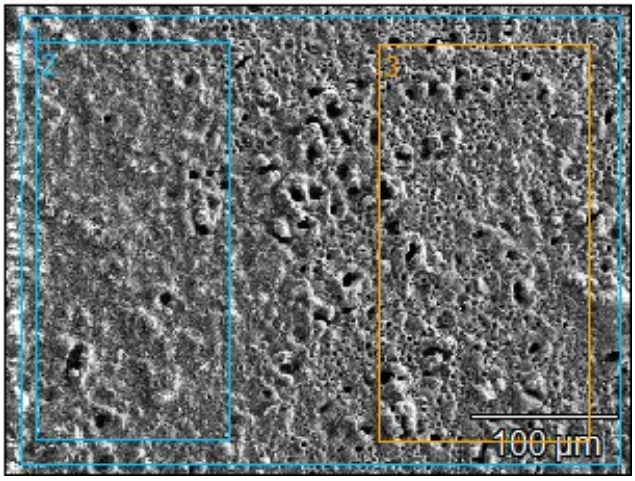


Figure 9.9 - 30 min phosphate post-conversion non uniform layer SEM image with 1)total of surface, 2) sealed porosity zone, 3) porous zone.

Table 9.3 -EDS results of the 30 min sample surface, pt 1,2,3 are referend to Figure 9.9.

	C-K	O-K	F-K	*Na-K*	*Mg-K*	Al-K	Si-K	*P-K*	Ca-K
F30,1 0h(1)_pt1	1.5	43.8	0.0	*9.1*	*25.6*	1.3	9.7	*8.4*	0.6
F30,1 0h(1)_pt2	1.4	46.2	0.1	*12.6*	*20.7*	1.0	7.8	*10.2*	--
F30,1 0h(1)_pt3	1.6	43.0	--	*6.9*	*28.8*	1.5	11.0	*6.6*	0.7

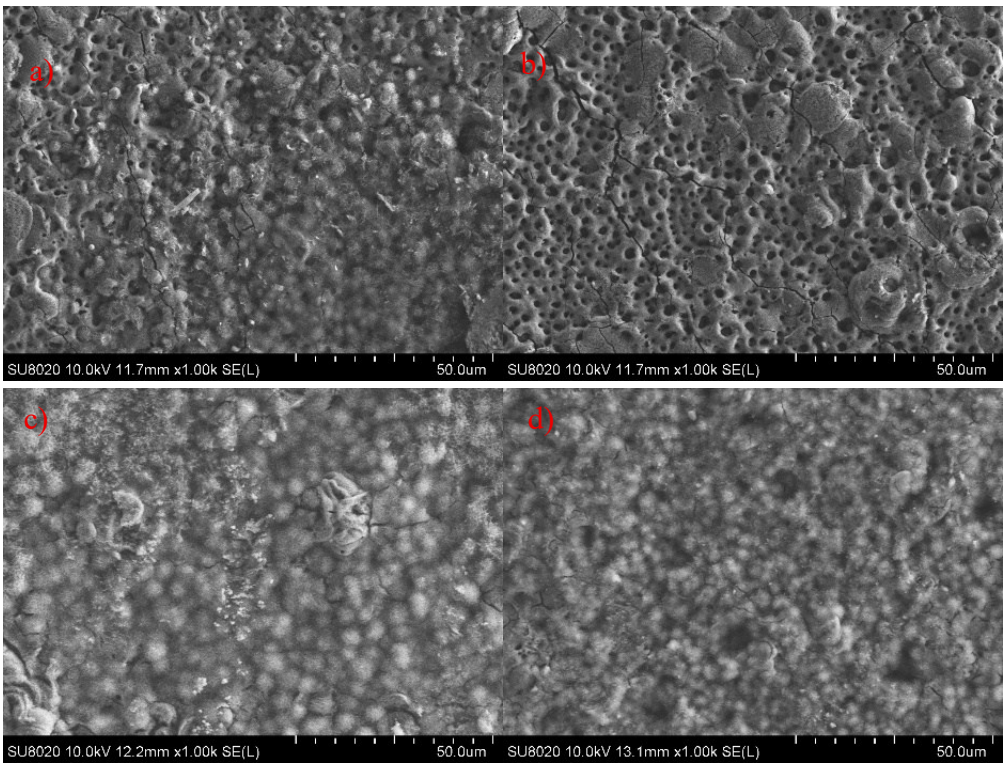


Figure 9.10 – Closed porosity by surfaces SEM images: a) 30 min of phosphate conversion pt1, b) 30 min of phosphate conversion pt2, c) 1h of phosphate conversion , d)2h of phosphate conversion.

The EDS analysis of the surfaces, reported in Table 9.2, shows that the specimens exhibit a certain degree of repeatability in their results. However, the 1-hour specimen displays a noticeably higher percentage of both P and Na compared to the other two. Phosphorus reaches 18.4 wt%, whereas in the 30-minute and 2-hour samples it remains at 15.4 wt% and 15.1 wt%, respectively.

As regards to the corroded samples, no significant differences were observed from the SEM and EDS analyses. As shown in Figure 9.11, the morphology of the deposited crystals does not appear to vary between the samples treated only with PEO and those subjected to PEO followed by phosphate post-conversion. However, compared to pure Mg shown in Figure 9.1, changes in both the crystal size and distribution can be observed.

By evaluating the elemental mapping in Figure 9.12, it can be observed that phosphorus, initially well distributed throughout the entire PEO layer with a higher concentration within the pores, becomes much more concentrated on the crystals after 24 hours of immersion, rather than being only superficially distributed. Furthermore, considering the data reported in Table 9.2, the repeatability of the results suggests that the corrosion products are mainly influenced by the corrosive medium rather than by the protective post-conversion layer. It is therefore interesting to evaluate the corrosion behaviour of the different systems investigated.

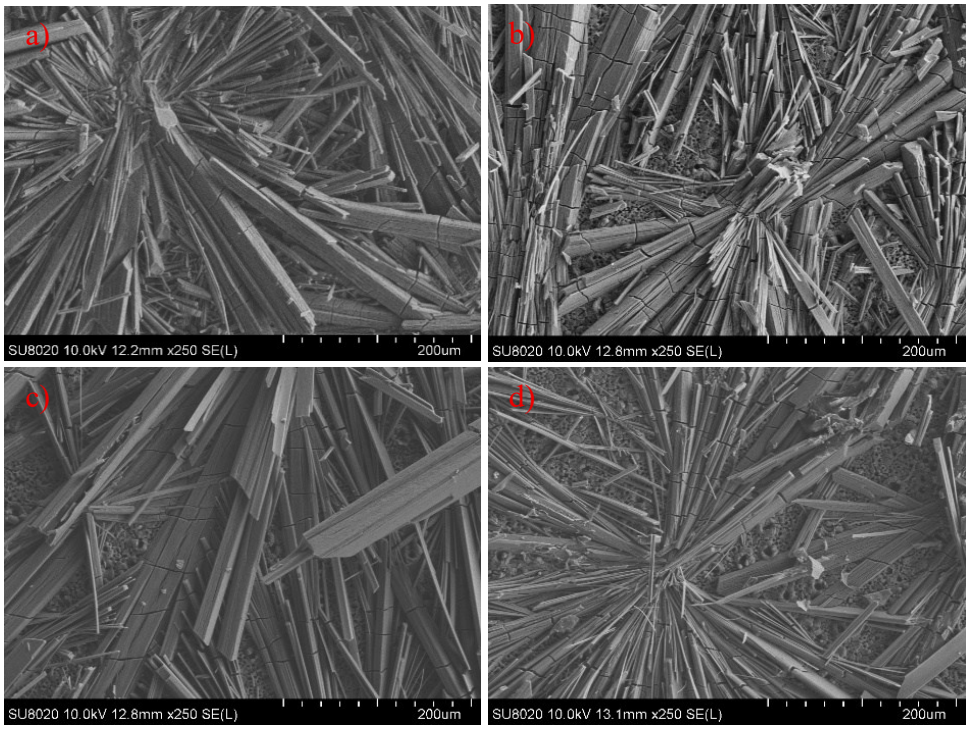


Figure 9.11 - Surfaces SEM images of 24h of immersion in PBS samples: a) PEO, b) 30 min phosphate post-conversion, c) 1h phosphate post-conversion, d) 2h phosphate post-conversion.

Summarizing, from the SEM and EDS analyses, it can be stated that the 30-minute phosphate treatment shows issues related to deposition uniformity, resulting in a thinner phosphate layer. In contrast, the 1-hour post-conversion treatment appears to provide the most effective and consistent deposition of the elements of interest.

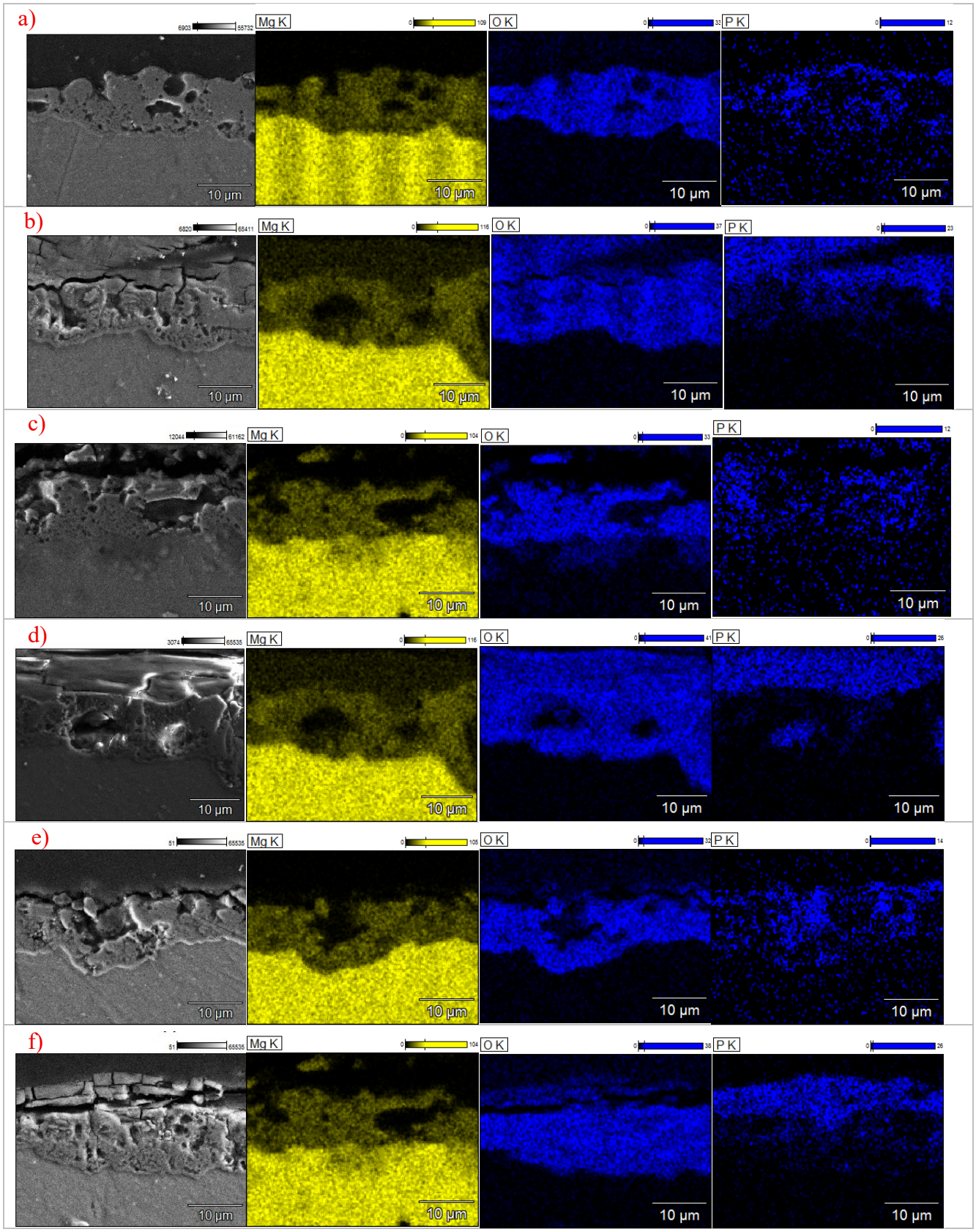


Figure 9.12 - EDS mapping of elements for samples a) 30 min phosphate conversion- before immersion in PBS, b) 30min phosphate conversion – after 24h of immersion in PBS, c) 1h phosphate conversion- before immersion in PBS, d) 1h phosphate conversion – after 24h of immersion in PBS, e) 2h phosphate conversion- before immersion in PBS, f) 2h phosphate conversion – after 24h of immersion in PBS.

Electrochemical impedance spectroscopy

Following the SEM analysis, the effectiveness of the deposited layers in terms of corrosion resistance was evaluated by means of electrochemical impedance spectroscopy (EIS). To establish a reference, an initial EIS analysis has been performed on the untreated AZ31 alloy and on samples treated by PEO deposition. The results are presented in Figure 9.13 and Figure 9.14. The bare AZ31 substrate exhibited the lowest impedance values, with low-frequency values below 3.2 × 10^3 Ω·cm², which further decreased over time, confirming its rapid and uncontrolled degradation in a physiological-like environment.

In contrast, the PEO-coated samples showed significantly enhanced corrosion resistance, reaching low-frequency impedance values of approximately 10^6 Ω·cm^2 (Figure 9.14) that remained relatively stable over the 24hour immersion period, indicating that the oxide layer effectively limits electrolyte penetration toward the magnesium substrate.

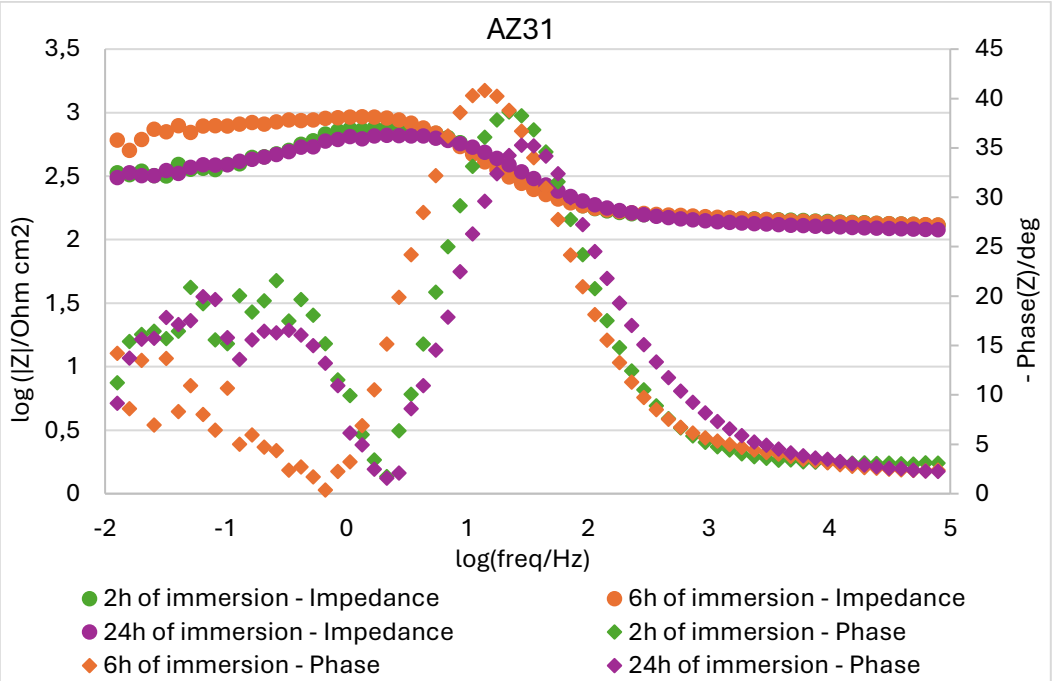


Figure 9.13 - Bare AZ31 EIS spectroscopy in function of the time of immersion in PBS.

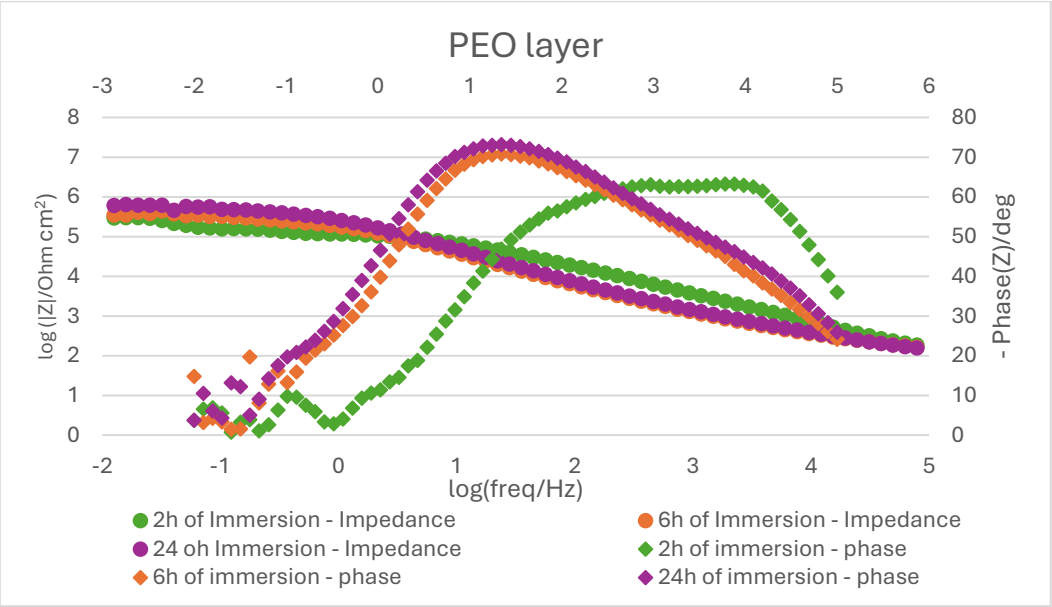


Figure 9.14 - AZ31 + PEO layer EIS spectroscopy results

The phosphate post-conversion samples (Figure 9.15Figure 9.15, Figure 9.16, Figure 9.17) exhibited higher corrosion resistance compared to the PEO layer alone, reaching an impedance modulus of approximately 3.7×10^{7} Ω·cm^2 at low frequencies. After 24 hours of immersion, however, the recorded impedance no longer showed significant differences among the samples. In all four cases (PEO and PEO + phosphate post-conversion), the impedance values were found to be around 3.2×10^{5} Ω·cm^2. More pronounced differences in corrosion resistance were observed after 6 hours of immersion, where different impedance values were measured among the three phosphate specimens.

After 6 hours of immersion, the differences become even more pronounced: the 30-minutes phosphate treated sample shows a marked decrease in impedance compared to the 1-hour and 2-hour counterparts, attributable to unsealed pores and surface defects that facilitate electrolyte penetration and the onset of localized corrosion. On the other side the 1hour and 2 hours treated samples maintain high impedance values and a well-defined capacitive behaviour, indicating stable and still effective protection of the metallic substrate.

After 24 hours, all three conditions converge towards the similar impedance values, suggesting that the outer layer has been partially degraded, that may be also observed in the SEM images of degraded sample after 24h of exposition (Figure 9.11 and Figure 9.12). Nevertheless, the phase angle analysis still reveals meaningful differences, as the 1 hour and 2 hour samples (respectively Figure 9.16 and Figure 9.17) retain a more defined maximum as an absolute value, indicating better integrity of the inner barrier layer, while the 30 minutes sample (Figure 9.15) shows a flatter curve, indicative of overlapping electrochemical processes and a more advanced degradation state.

The phase angle plots provide additional information regarding the evolution of the protective behaviour of the different phosphate post-conversion treatments during immersion in PBS. After 2 h

and 6 h of exposure, all three phosphate-treated samples exhibit two distinguishable time constants. This behaviour suggests the presence of two electrochemical processes occurring simultaneously: the high-frequency time constant can be associated with the outer porous phosphate/PEO layer, while the low-frequency contribution is related to the inner barrier layer and the charge transfer processes occurring at the metal/electrolyte interface. The presence of two well-defined time constants indicates that the protective coating system still maintains a multilayer behaviour and that the electrolyte has not yet fully penetrated the coating structure.

After 24 h of immersion, only one dominant time constant remains clearly visible for most samples, indicating progressive degradation of the outer layer and the increasing contribution of a single electrochemical process governing the corrosion behaviour. This evolution suggests that the distinction between the porous outer layer and the inner barrier layer becomes less pronounced as immersion time increases. Nevertheless, in the 1 h phosphate post-conversion sample, a slight shoulder can still be observed in the phase angle spectrum, suggesting that two partially distinguishable electrochemical responses may still be present. This behaviour indicates that the 1 h treatment retains a more stable layered structure compared to the 30 min and 2 h conditions, in agreement with the SEM, XRD, and impedance modulus results, which collectively identify the 1 h treatment as the most effective condition for corrosion protection.

Overall, the phosphate post-conversion treatment plays a crucial role in improving the protective properties of the PEO coating through the sealing of surface porosity, but its effectiveness strongly depends on treatment duration: 30 minutes proves insufficient to guarantee a uniform and durable coverage, while the 1- and 2-hours treatments offer superior and comparable performance. Based on these observations, the 30minute treatment was considered less reliable due to its early-stage instability.

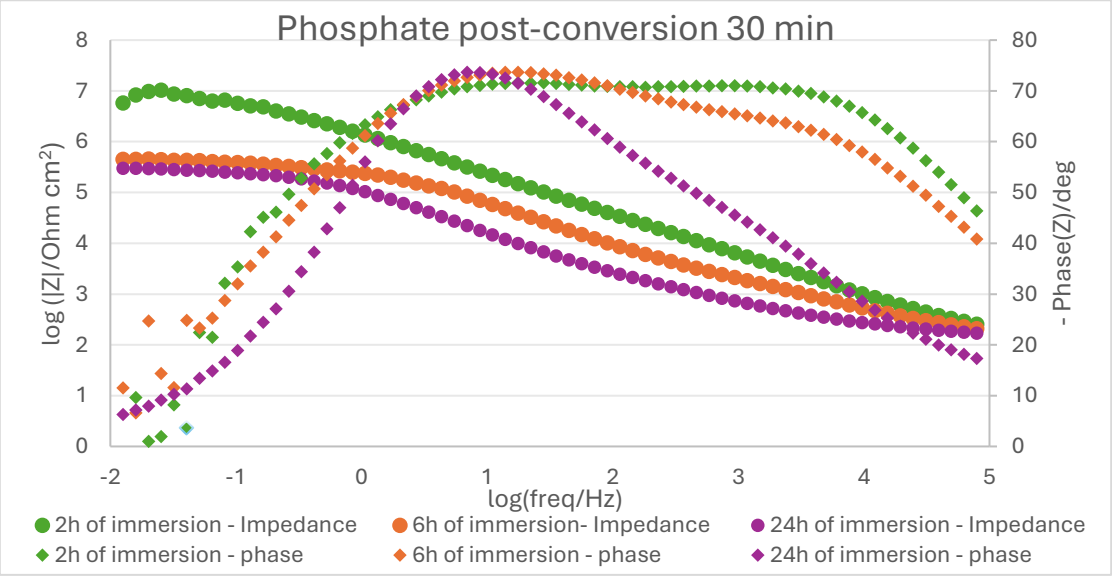


Figure 9.15 -Phosphate post-conversion 30 min EIS results.

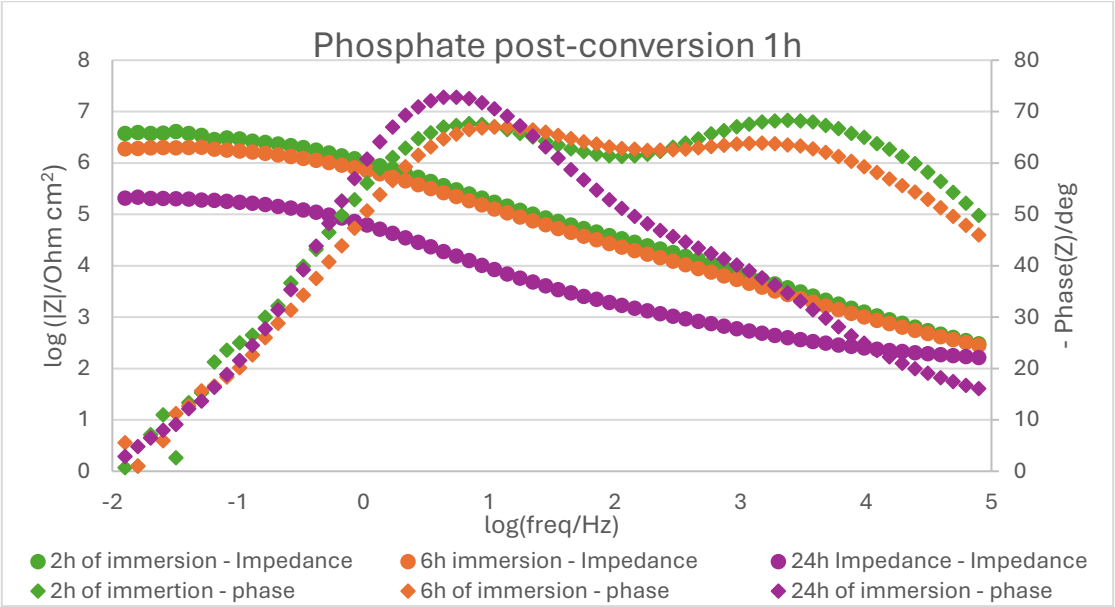


Figure 9.16 - Phosphate post-conversion 1h EIS results.

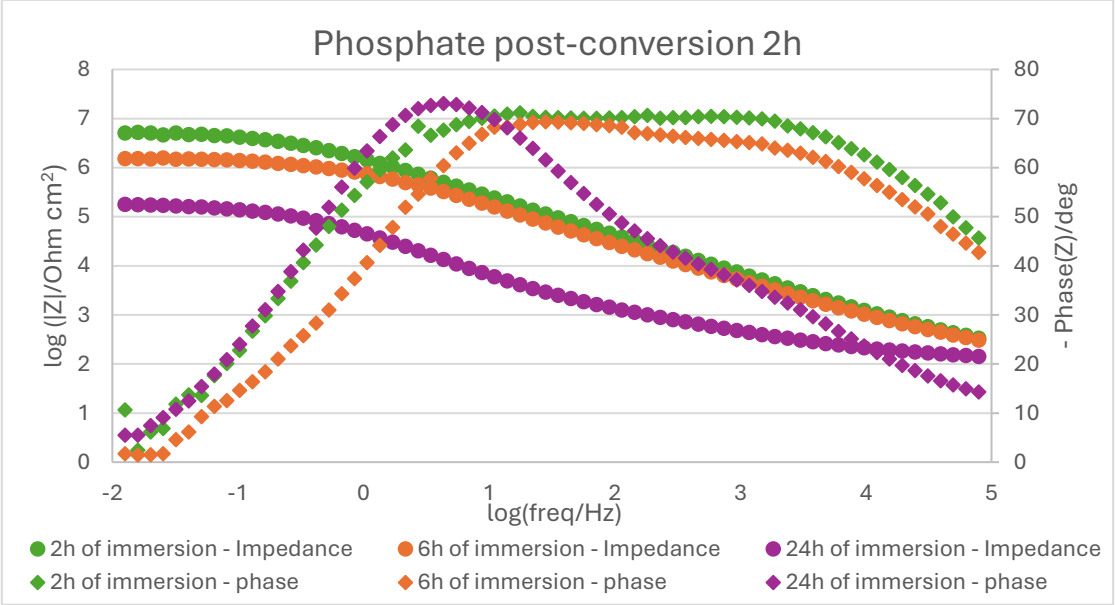


Figure 9.17 - Phosphate post-conversion 2h EIS results.

XRD Analysis results

X-ray diffraction analysis has been carried out in incidence mode (ω = 1°) to characterise the crystalline phases present in the PEO coating and in the post-conversion phosphate layers. The diffractograms obtained for the five conditions investigated (Bare AZ31, PEO, PEO + phospho 30 min, 1h, 2h) are shown in Figure 9.18.

The Bare AZ31 substrate exhibits intense and well-defined diffraction peaks characteristic of the Hexagonal Close-Packed (HCP) magnesium metal phase (Mg), located at their expected 2θ

positions[21],[33]. In all PEO-coated samples, the intensity of these Mg peaks is significantly reduced compared to the bare substrate, consistent with the formation of a ceramic oxide layer that attenuates the contribution of the underlying metal. This attenuation is particularly pronounced in the samples subjected to phosphate post-conversion treatment, reflecting the deposition of an additional surface layer on top of the PEO coating. In all coated samples, peaks attributable to MgO and Mg_2SiO_4 (forsterite) are clearly identifiable. The presence of Mg_2SiO_4 is consistent with the incorporation of silicate species from the electrolyte during the plasma discharge events of the PEO process.

Regarding the relative intensities of the identified phases across the different treatment conditions, no significant shift in peak positions is observed between the 30 minutes, 1 hour, and 2 hours phosphate post-conversion samples. This indicates that the overall crystalline phase composition of the PEO coating remains stable with increasing phosphate treatment duration, and with the conversion treatment no major modifications in the dominant crystalline phases are observed by XRD at this scale. Nevertheless, this observation does not exclude the formation of amorphous or poorly crystalline phosphate compounds in the outermost layer, which would be consistent with the significant increase in phosphorus content measured by EDS after immersion (Section 9.1) and with the needle-like morphology of the corrosion products observed by SEM.

In addition to the phases described above, several diffraction peaks at approximately 16.7°, 19.1°, and 30.05° 2θ are present exclusively in the diffractogram of the 1-hour phosphate post-conversion sample, and cannot be attributed to Mg, MgO, or Mg_2SiO_4. These additional low-angle reflections are associable with hydrated magnesium phosphate phases, particularly $MgHPO_4 \cdot xH_2O$ with x ranging from 0.5 to 7. Magnesium hydrogen phosphate hydrates ($MgHPO_4 \cdot xH_2O$) are considered weakly soluble in water, particularly under near-neutral conditions. The reported solubility product for $MgHPO_4 \cdot 3H_2O$ is $K_{sp} = 1.67 \times 10^{-6}$[41]. This could explain the improved corrosion resistance provided by the phosphate conversion layer on the PEO coating during the first hours of exposure to PBSA further assignment to other magnesium phosphate compounds, such as $Mg_3(PO_4)_2$ or struvite-type phases, cannot be excluded given the phosphate-rich environment of the conversion bath. A definitive identification of these reflections would require comparison with additional reference patterns and possibly complementary characterisation techniques such as Raman spectroscopy[42], [43].

The exclusive presence of these peaks in the 1 hour treated sample, and their absence in both the 30 minutes and 2 hours conditions, allows for a meaningful interpretation of the three treatment durations. The 30 minutes treatment appears insufficient to promote uniform and complete phosphate deposition, as also supported by the SEM observations showing partially sealed porosity and a non-homogeneous layer (Section 9.1). The absence of these reflections in the 2 hours sample may suggest,

considering also the solubility of $MgHPO_4 \cdot 3H_2O$, that prolonged exposure to the conversion bath promotes either partial redissolution of the newly formed phosphate phases or their further transformation into amorphous or differently structured compounds, reducing their crystalline detectability by XRD. The 1h treatment therefore appears to represent the optimal condition for the formation of a crystalline phosphate-rich layer on the PEO coating, in agreement with the EIS and SEM results discussed in precedent sections, which collectively identify this duration as the most effective for enhancing the corrosion resistance of the system.

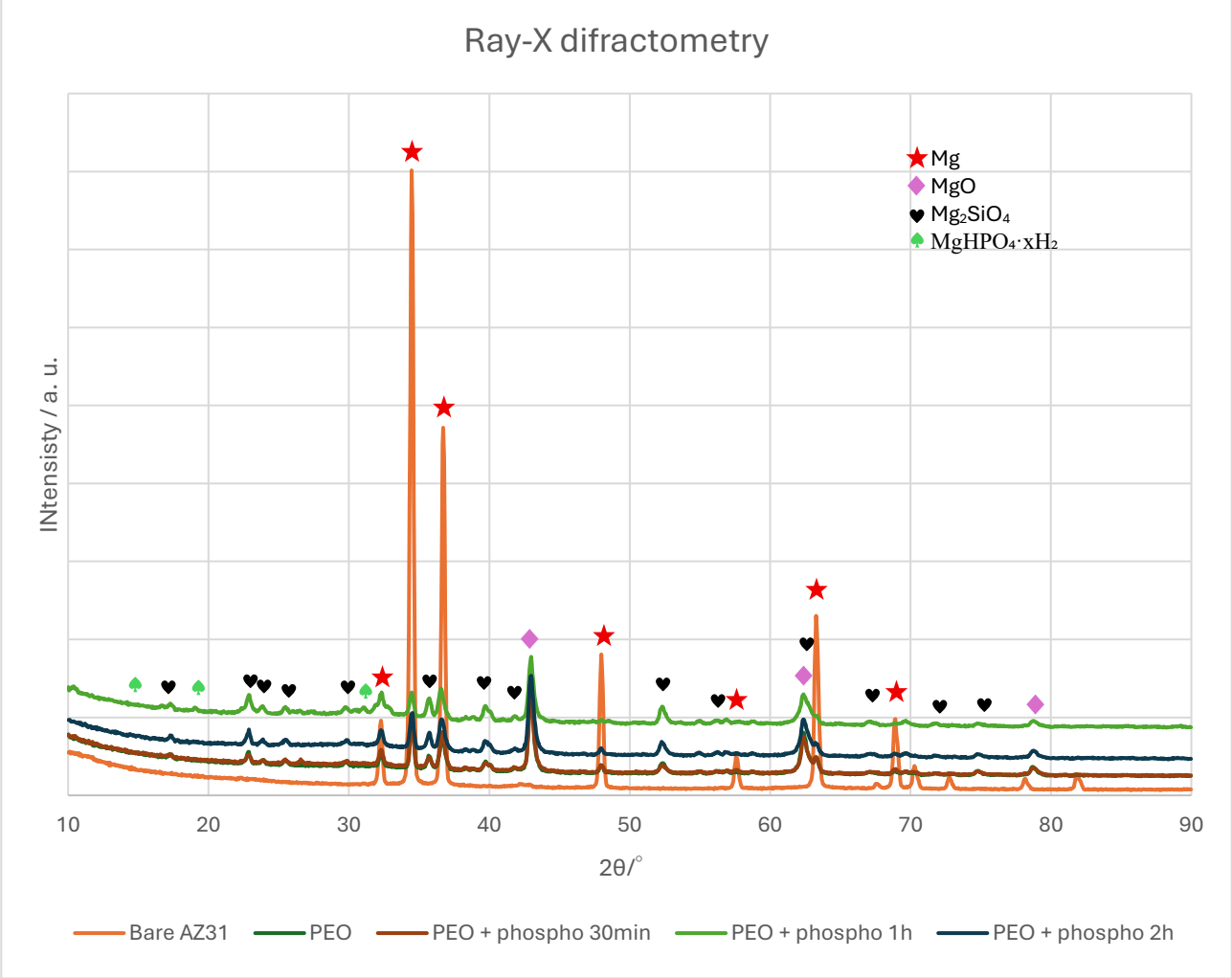


Figure 9.18 - X-ray diffractometry of different samples.

Summary of Characterization Results

Overall, the combined SEM, EDS, XRD, and EIS analyses highlighted the significant influence of the phosphate post-conversion treatment on the properties of the PEO-coated AZ31 alloy. SEM observations revealed progressive sealing of the PEO porosity after phosphate treatment, while EDS confirmed an increased phosphorus incorporation within the coating. XRD analyses indicated the possible formation of hydrated magnesium phosphate phases, particularly in the 1 h treated sample. Electrochemical measurements demonstrated an overall improvement in corrosion resistance for all

phosphate-treated specimens compared to the PEO layer alone, with the 1 h treatment showing the most stable and homogeneous behaviour throughout the immersion tests.

After 24 hours of exposure to the corrosive solution, all specimens exhibit comparable properties, indicating that the phosphate layer has already lost most of its protective efficacy by this stage. In contrast, EIS analysis reveals significant differences among the samples already after 6 hours of immersion, most notably for the 30-minute treated specimen, which shows a marked drop in corrosion resistance compared to the 1 h and 2 h conditions. Although these differences are no longer clearly distinguishable after 24 hours, their occurrence at early immersion times is relevant from a biomedical perspective. Indeed, the initial post-implantation period is characterized by an active inflammatory response. Previous studies have shown that inflammatory conditions can significantly affect the degradation behaviour of magnesium-based materials, with pro-inflammatory environments being associated with increased corrosion and surface degradation[44].

This early-stage improvement is consistent with previous studies on phosphate post-treatment of PEO-coated magnesium alloys, which have generally reported an improvement in corrosion resistance following the post-conversion treatment[45]. However, most of the available literature evaluates the corrosion behaviour at longer immersion times, typically after several days of exposure (e.g., 3–6 days)[44], [46]. In this context, the differences observed in the present study already after 6 hours are particularly relevant, as they provide information on the very early-stage behaviour of the coating. Although the differences between the samples become less pronounced after 24 hours, the results suggest that the beneficial effect of the phosphate post-treatment can be detected during the initial stages of immersion. Therefore, the present findings are broadly consistent with the overall improvement in corrosion resistance reported in the literature, while also highlighting the importance of investigating shorter immersion times. This is particularly relevant in the context of the present study, where the phosphate post-treatment is intended not only to improve corrosion resistance but also to functionalize the PEO surface for the subsequent loading of the anti-inflammatory drug.

9.2. SURFACE FUNCTIONALIZATION VIA BSP DRUG INCORPORATION

9.2.1. First set of deposition - Depos A to D

SEM-EDS Characterisation

Based on the results obtained in the previous section, the specimen treated with 1h phosphate post-conversion exhibited the most favourable overall performance. Therefore, although both the 1 h and 2 h conditions were investigated during the experimental phase, the following analysis focuses primarily on the 1 h treated samples, as they provided the most significant and representative results. The aim of these samples conditions was to evaluate two different solvents, methanol and distilled water, as deposition media for BSP through a dip-coating treatment. From the surface analysis,

reported in Figure 9.19, of *Ph1h_methAx3* (a) and *Ph1h_h2oCx3* (b) a significant difference is immediately evident. In fact, for *Ph1h_h2oCx3* (Figure 9.19-b) no distinct additional coating is visible above the PEO layer. Moreover, by examining Figure 9.20 and comparing it with Figure 9.7 and Figure 9.8, it can be stated that the layer formed during the post-treatment appears to have been removed or significantly reduced.

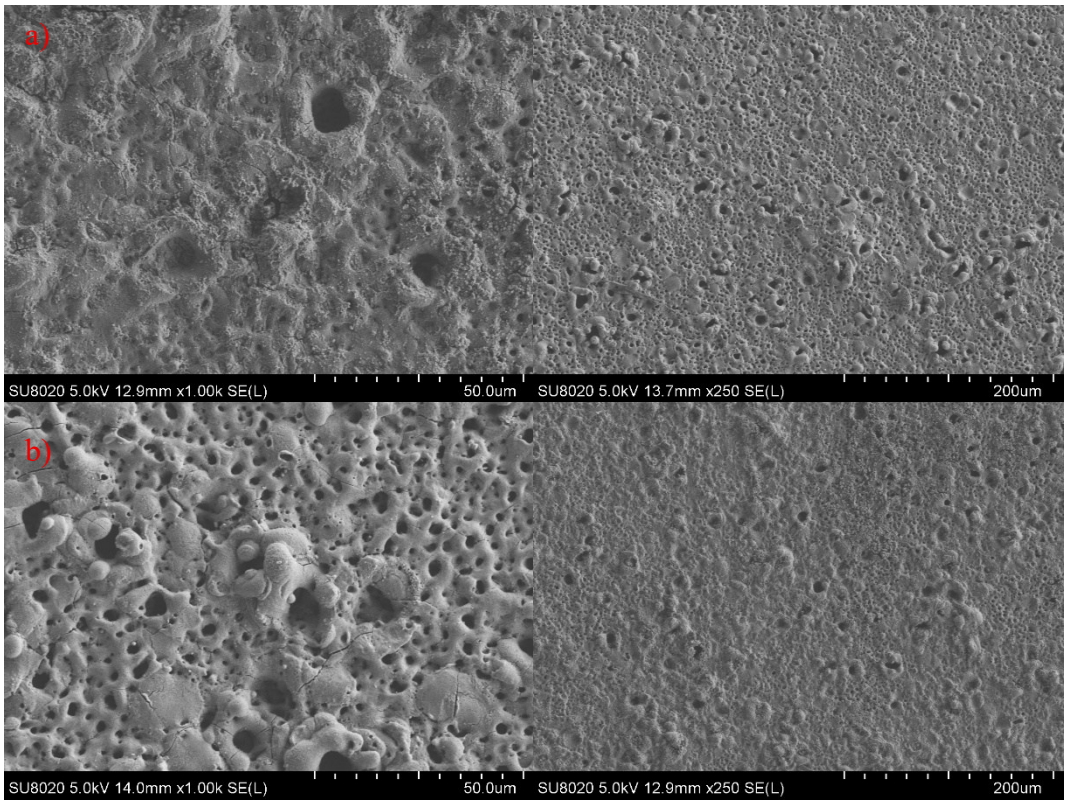


Figure 9.19 – SEM surface images of a) Ph1h_methAx3 and b) Ph1h_h2oCx3.

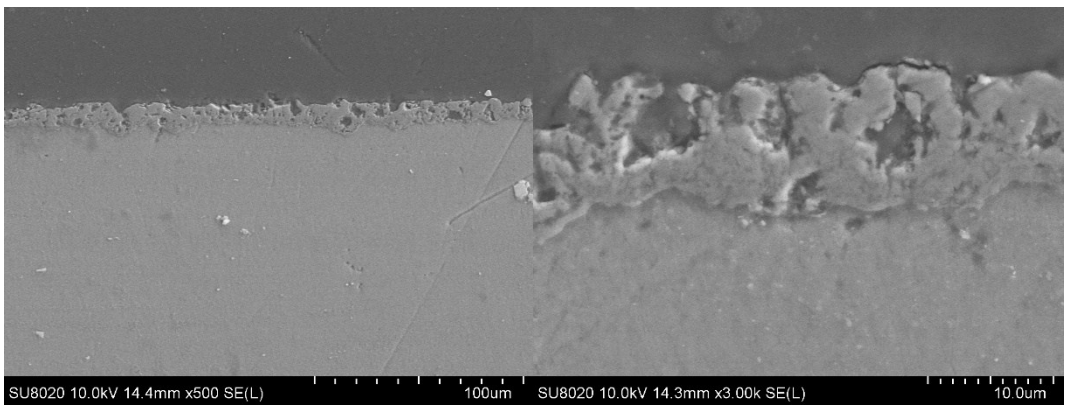


Figure 9.20 - Cross-section SEM image of Ph1h_h2oCx3.

Further surface EDS analysis (Table 9.4) revealed that the weight percentages of P and Na drastically decreased compared to the phosphate-treated samples. Nevertheless, a small residual amount is still detectable, confirming that the phosphate post-conversion treatment had been previously carried out. A decrease in the P and Na content compared to the values measured immediately after the phosphate post-conversion treatment was also observed for Ph1h_methAx3, treated with methanol. In this case,

however, the SEM image (Figure 9.19) reveals the presence of a superficial layer covering the porosities, with a morphology different from the one observed immediately after the post-conversion treatment. This feature could be associated either with a newly formed surface deposition or with a partial dissolution and reprecipitation of the phosphate layer occurred during the BSP deposition process.

Indeed, the SEM cross-sectional image shows that the presence of a layer above the PEO coating can still be identified, although it appears more fragmented compared to the condition prior to BSP deposition, suggesting partial modification of the phosphated layer during treatment.

Considering the solubility behaviour of hydrated magnesium phosphate compounds, such as newberyite ($MgHPO_4 \cdot 3H_2O$), in the two solvents employed, the observed behaviour appears consistent with the experimental results. Although the solubility of these compounds in water is relatively low, it is still significant enough to lead to a complete dissolution of the phosphate layer, under prolonged immersion and continuous stirring conditions for three times. In contrast, methanol, being an organic solvent, exhibits both higher volatility and a lower ability to solubilize hydrated magnesium phosphates, thereby limiting dissolution of the layer and allowing partial preservation of the surface coating.

Furthermore, considering that the drug is an organic molecule mainly composed of carbon, a higher carbon content would be expected from the EDS analysis, similar to the results reported by Bordbar-Khiabani et al.(*[28]*) , where carbon contents approaching 40wt% were measured. However, in the present case, the measured carbon percentage remained relatively low overall, although still higher in Ph1h_methAx3 (3.0 wt%) than in Ph1h_h2oCx3 (1.2 wt%). It should be noted that the quantitative analysis of light elements, including carbon, is challenging using EDS and may influence the measured composition. Consequently, the reported values should be interpreted with caution, since the uncertainty associated with EDS quantification is approximately 1 at.%, which is comparable to the differences observed between the samples.

Table 9.4 - EDS analysis of Ph1h_methAx3.

	C %wt	O %wt	F %wt	Na %wt	Mg %wt	Al %wt	Si %wt	P %wt	Ca %wt
Ph1h_methAx3 Surface	3.0	42.2	0.7	6.0	28.4	1.2	9.7	7.7	1.0
Ph1h_h2oCx3 Surface	1.2	41.8	0.5	1.4	35.8	1.6	12.8	3.4	1.4

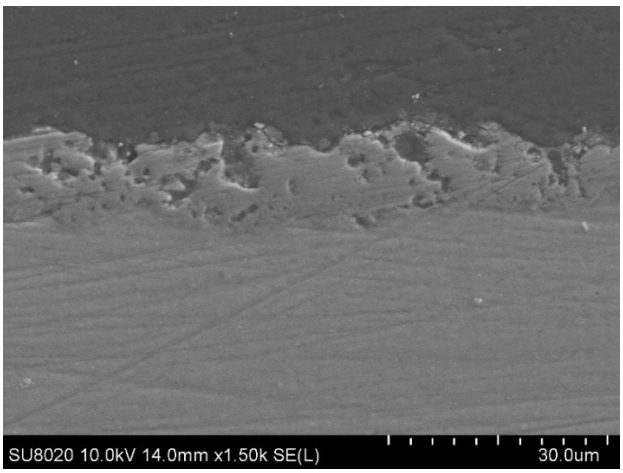


Figure 9.21 - Cross section SEM image of Ph1h_methAx3.

UV-Vis Results

The UV–Vis results do not provide clear evidence of a significant BSP release. The absorbance values measured at 242 nm are very low and do not show a distinct peak or a relevant increase compared to the baseline and neighbouring wavelengths. Therefore, the small fluctuations observed over time are likely attributable to instrumental noise, baseline variations or experimental uncertainty rather than to an actual measurable release. Moreover, since the measured concentrations fall in the low concentration/non-linear region of the calibration curve, the quantitative values obtained should be considered unreliable or only semi-quantitative.

Table 9.5 - UV-Vis spectroscopy absorbance results for Ph1h_methAx3 to D.

	Ph1h_methAx3	*Ph1h_h2oCx3*
2h	0.0249	0.0117
6h	0.0252	0
24h	0.0276	0.0007
48h	0.0322	0.0132
5gg	0.0441	0.0983
6gg	0.0548	0.0488
7gg	0.0572	0.1293

Summary of characterization Results

Overall, the results do not allow a definitive confirmation of successful BSP deposition. SEM observations suggest that the treatment modified the surface differently depending on the solvent: *Ph1h_h2oCx3* showed a dissolution or removal of the phosphate layer, whereas *Ph1h_methAx3* retained

a partially preserved superficial layer that could be related either to BSP deposition or to phosphate reprecipitation phenomena.

EDS analysis showed only a limited increase in carbon content, significantly lower than values reported in the literature for successful BSP incorporation. Moreover, UV–Vis measurements did not show clear evidence of BSP release, since the absorbance values remained very low and close to the baseline noise level. Therefore, the observed variations are likely associated with experimental uncertainty rather than with a significant release phenomenon.

Overall, the combined results remain inconclusive regarding the effective deposition of BSP under the investigated conditions.

9.2.2. Second set of deposition – Depos 1 to 10

SEM-EDS Characterisation

Since the results discussed in Section 10.2.1 suggested that a possible limitation of the process was related to the solubility of the phosphate conversion layer compounds and the partial dissolution of the coating during multiple immersions may have occurred. This phenomenon could reduce the availability of phosphate species and surface hydroxyl groups potentially involved weak interactions, including possible hydrogen bonding between BSP molecules and the substrate, thereby limiting the effective retention of the drug on the surface.

Based on these considerations, the number of deposition/drying cycles was reduced to one, leading to the production of samples with methanol (*8_Ph91h_PBS_meth_BSPx18)* and distilled water (*9_Ph91h_PBS_h2o_BSPx1)* like solvent.

In this case, SEM observations did not reveal major differences between the two systems. Indeed, for both samples, a superficial layer filling the coating porosities was still visible Figure 9.21, with a comparable thickness in the two conditions Figure 9.22.

EDS analysis showed an increase in the P and Na contents compared to *Ph1h_methAx3* and *Ph1h_h2oCx3* (Table 9.6). The concentration of both elements was higher in *8_Ph91h_PBS_meth_BSPx1* than in *9_Ph91h_PBS_h2o_BSPx1*, where the values were comparable to those measured after the phosphate post-conversion treatment alone (Table 9.2). However, the carbon percentage remained relatively low compared to the values expected from literature data.

Table 9.6 - - EDS analysis of 8_Ph91h_PBS_meth_BSPx1 and 9_Ph91h_PBS_h2o_BSPx1.

	C %wt	O %wt	Na %wt	Mg %wt	Al %wt	Si %wt	P %wt	Ca %wt
8_Ph91h_PBS_meth_BSPx1 Surface	0.9	48.7	14.6	13.9	0.3	2.6	18.9	--
9_Ph91h_PBS_h2o_BSPx1 Surface	1.9	46.5	1.6	27.4	1.2	6.2	11.8	3.5

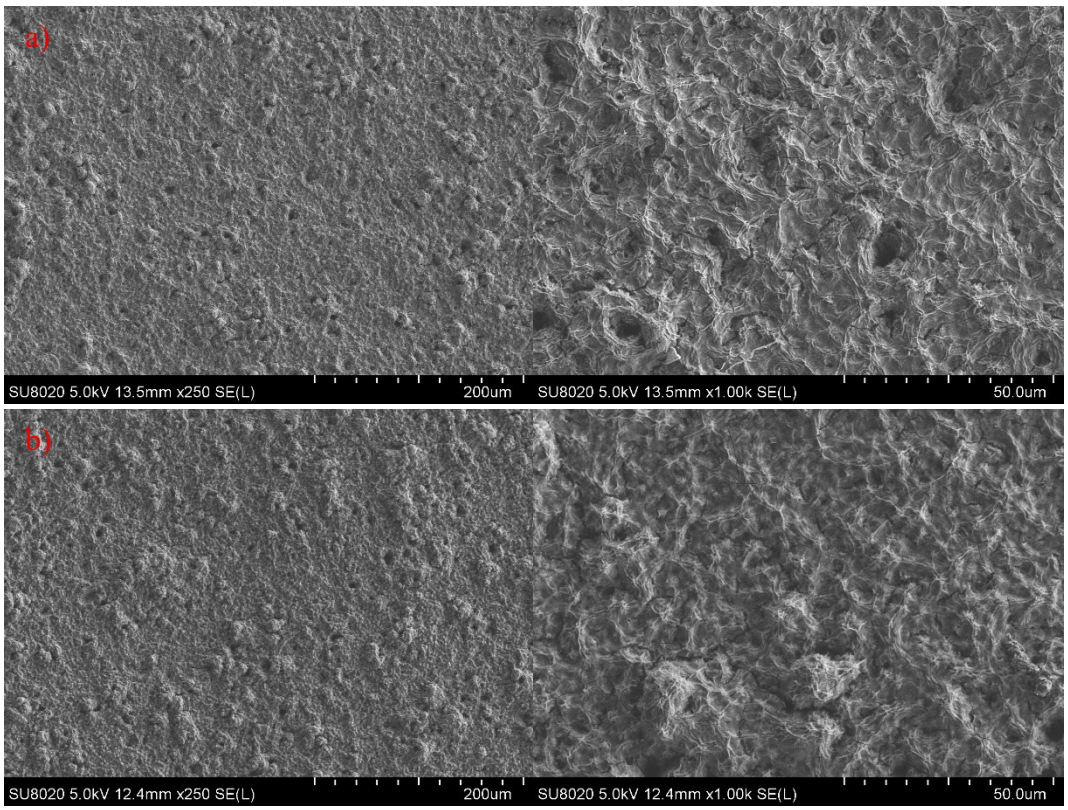


Figure 9.21 - Surface SEM image of a) 8_Ph91h_PBS_meth_BSPx1 and b) 9_Ph91h_PBS_h2o_BSPx1.

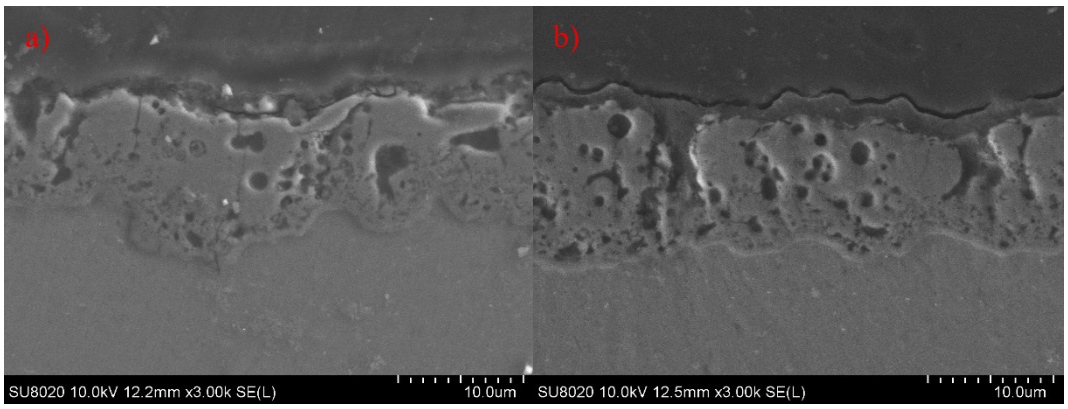


Figure 9.22 – Cross-section SEM image of a) 8_Ph91h_PBS_meth_BSPx1 and b) 9_Ph91h_PBS_h2o_BSPx1.

Considering the improved results, although the amount of drug associated with the carbon percentage was still lower than expected, further modifications of the deposition protocol were investigated for both solvents.

For the methanol-based system, the dip-coating approach was replaced by a drop casting technique. After preparing the BSP solution in methanol, droplets were uniformly distributed over the sample surface using a Pasteur pipette. The solvent was allowed to evaporate completely before the deposition procedure was repeated five times to obtain the desired coating. The obtained results were overall similar to those previously observed. SEM images appeared fully comparable to those obtained for *8_Ph91h_PBS_meth_BSPx1*, showing the presence of a superficial layer covering the coating porosities. A slight difference could be observed in the morphology of the deposited layer in

the cross-sectional images (Figure 9.23), most likely related to solvent evaporation during the dropping process. However, at this stage of the analysis, this difference does not allow a clear assessment of whether the deposition effectiveness was improved. EDS analysis in Table 9.8 revealed slightly lower P and Na contents compared to *8_Ph91h_PBS_meth_BSPx1*, although both elements were still present in significant amounts.

Table 9.7 - EDS results for 6_Ph91h_meth_PBS_drop.

	C %wt	O %wt	Na %wt	Mg %wt	Al %wt	Si %wt	P %wt
6_Ph91h_meth_PBS_drop Surface	1.4	45.1	9.6	21.5	0.7	5.7	15.9

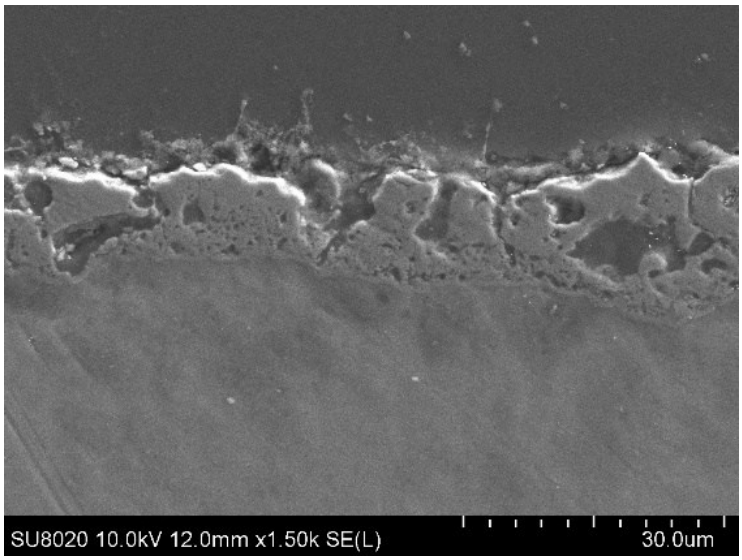


Figure 9.23 - Cross-section SEM image of 6_Ph91h_meth_PBS_drop.

For the aqueous-based deposition system, whose protocol modifications were discussed in more detail in Section 9.2.2, the obtained results were less promising. In both *8_Ph91h_PBS_acqu_BSPx1* and *1_Ph91h_acq_PBS_eth*, the phosphated layer appeared to be partially removed, leading to the re-exposure of the coating porosities. This behaviour may be associated with the increased number of immersion and drying treatments, which could promote progressive dissolution of the newberyite-based layer, even when shorter immersion times were employed.

Furthermore, the presence of H_3PO_4 in the BSP-containing solution may have promoted interactions between the two compounds. However, no specific studies addressing this phenomenon were found in the available literature. Therefore, a proper evaluation of such possible interactions would require the use of additional analytical techniques, such as FTIR, XPS or Raman spectroscopy.

This hypothesis may be further supported by the results obtained for sample *2_ph8T40_BSPinPhosp*, in which BSP was directly dissolved in the phosphate post-conversion solution. As shown in Figure 9.24, a partial surface deposition can still be observed, although the morphology and continuity of the

layer are not comparable with those obtained in Section 9.1 for the phosphate-treated samples without BSP addition.

Dissolving BSP directly in the H_3PO_4/NaOH post-conversion solution could promote its in situ incorporation within the growing magnesium phosphate layer. In this case, BSP would not simply be deposited onto a pre-formed coating but could become physically entrapped or weakly coordinated with Mg^{2+} species during phosphate precipitation. However, the presence of BSP may also interfere with the nucleation and growth of newbarryite, which reaction of formation is reported in equations 9 to 13, potentially affecting coating morphology, composition and stability. Therefore, although this approach appears promising, further experimental validation and additional chemical characterization techniques would be required to better clarify the effective interactions occurring within the system [25], [26], [47].

$$MgO + H_2O \rightarrow Mg(OH)_2 \quad (9)$$

$$2H^+ + 2e^- \rightarrow H_2 \quad (10)$$

$$H_2PO_4^- + H^+ \leftrightarrow HPO_4^{2-} + 2H^+ \quad (11)$$

$$Mg(OH)_2 + 2H_3PO_4 \rightarrow Mg(H_2PO_4)_2 + 2H_2O \quad (12)$$

$$Mg^{2+} + H_2PO_4^- + 3H_2O \rightarrow MgHPO_4 \cdot 3H_2O + H^+ \quad (13)$$

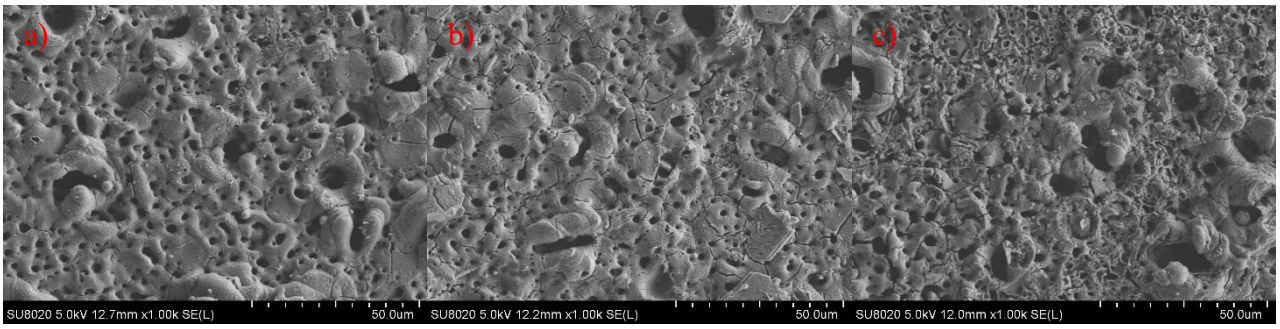


Figure 9.24 - Surface SEM image of a) 1_Ph91h_acq_PBS_eth ,b) 8_Ph91h_PBS_acqu_BSPx1 and c) 2_ph8T40_BSPinPhosp.

For sample *2_ph8T40_BSPinPhosp*, the effective formation of the phosphate layer could be questioned due to the modified processing conditions adopted to preserve the drug. Therefore, sample 3*_ph8T401h_acqu_BSP_eth* was further investigated to evaluate the reliability of the obtained results (Figure 9.25).

In 3*_ph8T401h_acqu_BSP_eth*, the formation of a superficial deposited layer was again observed. EDS analysis, reported in Table 9.9 revealed a phosphorus content of 9.3 wt%, corresponding to a lower value compared to *8_Ph91h_PBS_meth_BSPx1*, *9_Ph91h_PBS_h2o_BSPx1* and *6_Ph91h_meth_PBS_drop*, but still higher than the values measured for *Ph1h_methAx3* and *Ph1h_h2oCx3*. The results obtained from the other deposition protocols did not provide any significant or distinctive findings to justify a detailed discussion.

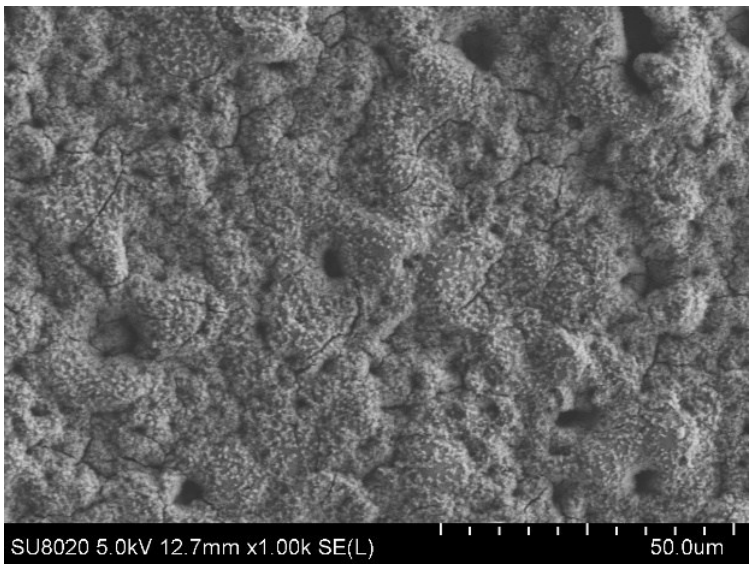


Figure 9.25 - Surface SEM image of 3_ph8T401h_acqu_BSP_eth.

Table 9.9 -EDS results for 2_ph8T40_BSPinPhosp and 3_ph8T401h_acqu_BSP_eth.

	C %wt	O %wt	F %wt	Na %wt	Mg %wt	Al %wt	Si %wt	P %wt
2_ph8T40_BSPinPhosp Surface	0.6	43.0	0.2	5.8	22.1	2.8	12.6	11.1
3*_ph8T401h_acqu_BSP_eth* Surface	0.9	47.6	0.3	1.6	23.1	2.7	12.6	9.3

UV-Vis Results

According to the calibration curve in Figure 8.2, which the reference is the Equation 14, most of the measured absorbance values were lower than the intercept of the calibration line (see Table 9.10), indicating that the detected signals were below the reliable quantification range of the UV–Vis method.

$$y = 1{,}05 \cdot 10^{4}\, x + 0{,}114 \tag{14}$$

Therefore, the obtained measurements cannot be considered as quantitative evidence of a significant BSP release, and the observed variations are more likely attributable to baseline fluctuations and experimental uncertainty. This can also be observed in Figure 9.26, where the UV–Vis spectra of *8_Ph91h_PBS_meth_BSPx1* after 7 days (corresponding to the sample with the highest measured absorbance) and *1_Ph91h_acq_PBS_eth* after 6 days (one of the samples showing the lowest absorbance values throughout the entire analysis) are compared with the spectrum of the PEO sample without BSP deposition. The spectra exhibit an almost overlapping behaviour, and the observed differences are too small to be considered reliable evidence of a significant BSP release. To further assess whether BSP was effectively deposited onto the surface, additional characterization techniques would be required. In particular, FTIR or Raman spectroscopy could be used to identify the characteristic functional groups of BSP, while XPS analysis could provide more detailed information on the surface chemical composition and possible interactions between BSP and the phosphate layer.

Moreover, HPLC analysis of the release medium could allow a more selective and sensitive quantification of BSP compared to UV–Vis spectroscopy, reducing the influence of baseline fluctuations or overlapping absorbance signals.

Table 9.10 - UV-Vis spectroscopy results for depos 1 to 10.

	PEO	*1_Ph9 1h_acq_PBS_eth*	*2_ph8 T40_BSPinPhosp*	*3_ph8 T401h_acqu_BSP_eth*	*4_ph8 T402h_acqu_BSP_eth*	*K_3PO_4 PEO_acqu_BSP_eth*	*6_Ph9 1h_meth_PBS_drop*	*7_Ph5_PBS_acqu_BSP*	*8_Ph9 1h_PBS_meth_BSPx1*	*9_Ph9 1h_PBS_h2o_BSPx1*	*10_Ph9 1h_PBS_acqu_BSPx1*
2h	0	0.0053	0.0059	0.0077	0.0091	0.0092	0.0148	0.0036	0.0118	0.0012	0
6h	0	0.0054	0.0075	0.0062	0.0115	0.009	0.0158	0.0064	0.0155	0.0064	0
24h	0	0.0067	0.0111	0.0113	0.0038	0.0129	0.0283	0.0154	0.0378	0.016	0
48h	0.0135	0.0119	0.018	0.0115	0.0188	0.0164	0.0299	0.0108	0.0336	0.0071	0.0076
3gg	--	--	--	0.0196	0.0279	0.0175	--	0.0008	0.034	0.0069	--
4gg	--	--	--	0.0184	0.0259	0.0135	--	--	--	--	--
5gg	0.014	--	--	--	--	--	0.0295	--	--	--	0.0084
6gg	0.0117	0.0136	0.0353	--	--	--	0.033	0.0154	0.048	0.0128	0.0073
7gg	0.0136	0.0118	0.0199	0.023	0.0313	0.0148	0.0291	0.0131	0.0275	0.0089	0.007

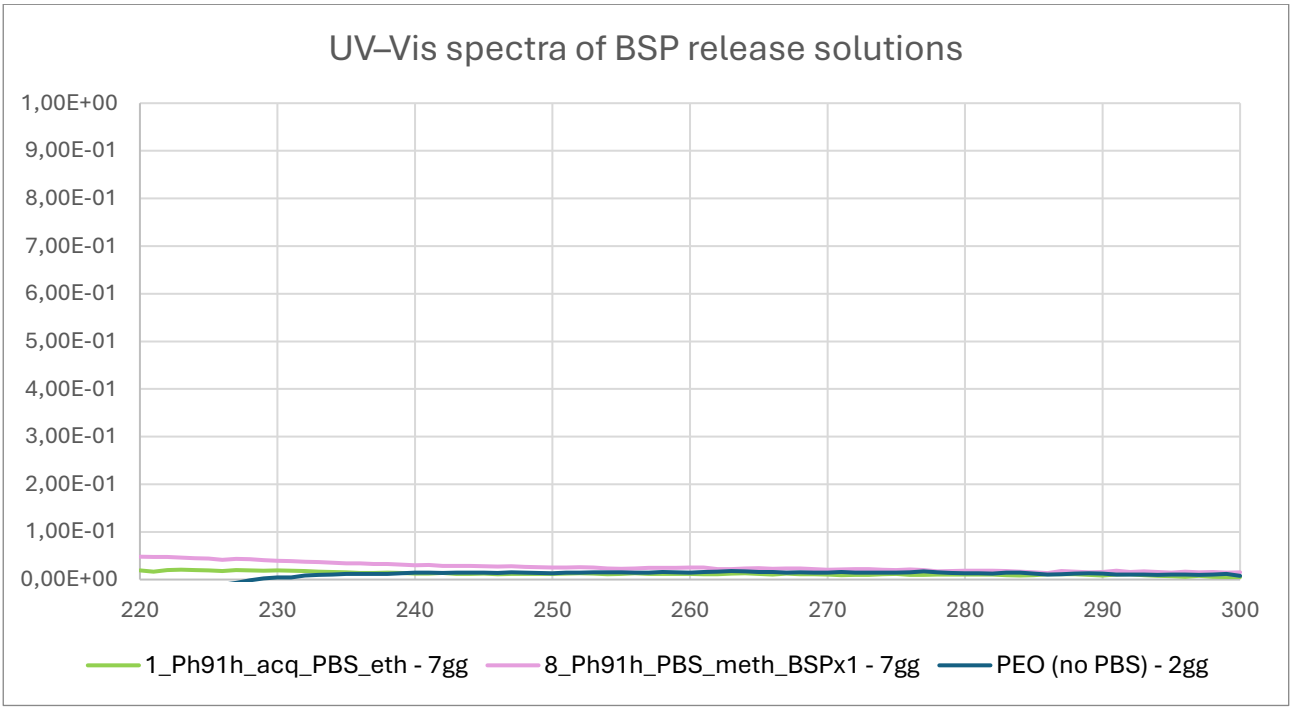


Figure 9.26 - UV-Vis spectra of PBS release solution for samples Depos1 and Depos8 after respectively 6 and 7 days of immersion, and sample PEO without BSP deposition after 2 days of immersion in PBS.

Summary of Characterization Results

In general, it has been found that reducing the number of deposition cycles led to a better preservation of the superficial phosphate layer, particularly for the methanol-based systems, where SEM observations showed the presence of a deposited layer partially filling the coating porosities. EDS analyses revealed higher P and Na contents compared to the first deposition attempts, although the measured carbon percentages remained lower than expected from literature data [28].

Additional modifications, including drop-coating deposition and BSP incorporation directly into the phosphate post-conversion solution, were also evaluated. While some surface modifications were observed, the obtained morphologies and compositions varied depending on the deposition conditions and solvent employed. UV–Vis analyses did not provide clear evidence of significant BSP release, since the measured absorbance values remained very close to the baseline and within the experimental uncertainty range.

10. CONCLUSIONS

The aim of this research was to optimize the corrosion resistance of PEO-treated AZ31 magnesium alloy through a dual approach: the deposition of a protective phosphate post-conversion coating, for which the optimal treatment duration (30 minutes, 1 hour, and 2 hours) was investigated, and the subsequent incorporation of the anti-inflammatory drug Betamethasone Sodium Phosphate (BSP) onto the modified surface.

The first phase of the study focused on the analysis of the phosphate layer deposition as a function of treatment time. SEM observations revealed a clear difference between the 30-minute treatment and the longer treatment durations. After 30 minutes the phosphate layer did not achieve homogeneous coverage over the entire surface and appeared thinner above the PEO structure. This treatment duration proved insufficient to ensure the formation of a continuous and uniform phosphate coating, as confirmed by the non-homogeneous elemental distribution observed by EDS analysis and by the lower impedance values measured during the early stages of immersion in PBS.

On the other hand, the 2-hour treatment, although morphologically very similar to the 1-hour condition, did not provide any significant advantages and even appeared to promote the initial re-dissolution of some phosphate compounds. Indeed, XRD analysis revealed that only the 1-hour treated sample showed distinct diffraction peaks attributable to hydrated magnesium phosphate compounds ($MgHPO_4 \cdot xH_2O$).

Regarding corrosion resistance, investigated by Electrochemical Impedance Spectroscopy (EIS), all three phosphate-treated samples exhibited a relatively similar behaviour after 2 h and 24 h of immersion in PBS. However, a significant difference was observed after 6 h, when the 30-minute sample showed a marked decrease in low-frequency impedance resistance, a behaviour not observed for the other two conditions. Once again, the 1-hour treatment exhibited the most favourable performance, as it preserved the two time constants associated with the corrosion resistance of both the inner barrier layer and the porous outer layer more clearly than the other samples, although one of them became significantly attenuated after 24 h of immersion.

The conclusions regarding drug incorporation are less definitive. The results mainly highlighted the sensitivity of the previously deposited phosphate layer to the different deposition procedures and solvents employed, rather than providing conclusive evidence of successful BSP incorporation. In particular, the Na–P layer, especially $MgHPO_4 \cdot xH_2O$, appeared highly sensitive to repeated immersion/drying cycles and to the deposition solvents. Distilled water showed a more aggressive behaviour toward the phosphate coating compared to methanol. Reducing the number of deposition cycles resulted in a partial improvement in surface preservation.

Nevertheless, EDS analyses consistently revealed carbon contents significantly lower than those reported in the literature for confirmed BSP incorporation, while UV–Vis spectroscopy did not provide clear evidence of significant drug release. The measured absorbance values remained within the baseline noise level throughout the entire immersion period.

Overall, the obtained results suggest that BSP may have been present on the surface in quantities below the detection limit of the employed techniques, or that the interactions between the drug and

the phosphate/PEO surface were too weak to ensure stable retention and subsequent controlled release under the investigated conditions.

10.1. FUTURE PERSPECTIVE

Given the limited success achieved during the drug deposition stage and considering that the primary cause of these unsatisfactory results is likely the poor mechanical stability and weak adhesion of the phosphate coating, future work should first focus on a more comprehensive investigation of the coating's physical, chemical, and mechanical properties. A deeper understanding of these characteristics is essential to optimize the coating and improve its performance as a drug carrier. Once a more robust phosphate layer has been developed, further studies should address the drug deposition process itself. This could include increasing the drug concentration in the deposition solution to enhance loading efficiency, as well as promoting stronger chemical interactions between the substrate, the phosphate coating, and the drug. For instance, the incorporation of divalent magnesium ions (Mg^{2+}) into the deposition system could be explored, as their ability to form stronger electrostatic interactions may improve the adhesion and stability of both the phosphate layer and the deposited drug.

BIBLIOGRAPHY

[1] M. Esmaeili, M. Tadayonsaidi, and B. Ghorbanian, 'The effect of PEO parameters on the properties of biodegradable Mg alloys: a review', *Surface Innovations*, vol. 9, no. 4, pp. 184–198, Aug. 2021, doi: 10.1680/jsuin.20.00057.

[2] E. Matykina *et al.*, 'Role of PEO coatings in long-term biodegradation of a Mg alloy', *Applied Surface Science*, vol. 389, pp. 810–823, Dec. 2016, doi: 10.1016/j.apsusc.2016.08.005.

[3] F. Witte *et al.*, 'Degradable biomaterials based on magnesium corrosion', *Current Opinion in Solid State and Materials Science*, vol. 12, no. 5–6, pp. 63–72, Oct. 2008, doi: 10.1016/j.cossms.2009.04.001.

[4] D. Zhao, F. Witte, F. Lu, J. Wang, J. Li, and L. Qin, 'Current status on clinical applications of magnesium-based orthopaedic implants: A review from clinical translational perspective', *Biomaterials*, vol. 112, pp. 287–302, Jan. 2017, doi: 10.1016/j.biomaterials.2016.10.017.

[5] A. Atrens, G.-L. Song, F. Cao, Z. Shi, and P. K. Bowen, 'Advances in Mg corrosion and research suggestions', *Journal of Magnesium and Alloys*, vol. 1, no. 3, pp. 177–200, Sep. 2013, doi: 10.1016/j.jma.2013.09.003.

[6] L. Y. He, X. M. Zhang, B. Liu, Y. Tian, and W. H. Ma, 'Effect of magnesium ion on human osteoblast activity', *Braz J Med Biol Res*, vol. 49, no. 7, p. e5257, 2016, doi: 10.1590/1414-431x20165257.

[7] S. Castiglioni, A. Cazzaniga, W. Albisetti, and J. Maier, 'Magnesium and Osteoporosis: Current State of Knowledge and Future Research Directions', *Nutrients*, vol. 5, no. 8, pp. 3022–3033, Jul. 2013, doi: 10.3390/nu5083022.

[8] L. Meng *et al.*, 'Comparative Investigation of the Corrosion Behavior and Biocompatibility of the Different Chemical Conversion Coatings on the Magnesium Alloy Surfaces', *Metals*, vol. 12, no. 10, p. 1644, Sep. 2022, doi: 10.3390/met12101644.

[9] Y. Xin, T. Hu, and P. K. Chu, 'In vitro studies of biomedical magnesium alloys in a simulated physiological environment: A review', *Acta Biomaterialia*, vol. 7, no. 4, pp. 1452–1459, Apr. 2011, doi: 10.1016/j.actbio.2010.12.004.

[10] J. Liang, P. B. Srinivasan, C. Blawert, and W. Dietzel, 'Influence of pH on the deterioration of plasma electrolytic oxidation coated AM50 magnesium alloy in NaCl solutions', *Corrosion Science*, vol. 52, no. 2, pp. 540–547, Feb. 2010, doi: 10.1016/j.corsci.2009.10.011.

[11] D. Mei, S. V. Lamaka, X. Lu, and M. L. Zheludkevich, 'Selecting medium for corrosion testing of bioabsorbable magnesium and other metals – A critical review', *Corrosion Science*, vol. 171, p. 108722, Jul. 2020, doi: 10.1016/j.corsci.2020.108722.

[12] Stephen C. Cowin, *Bone Mechanics Handbook*, 2001st edn. CRC Press.

[13] S. Feliu, 'Electrochemical Impedance Spectroscopy for the Measurement of the Corrosion Rate of Magnesium Alloys: Brief Review and Challenges', *Metals*, vol. 10, no. 6, p. 775, Jun. 2020, doi: 10.3390/met10060775.

[14] I. Tournay-Dufrenne, C. Pasté, A. Mégret, L. Dangreau, and M.-G. Olivier, 'Effect of the Fluoride Species and Content of the PEO Electrolyte on the Corrosion Properties of the Layers Obtained on AZ31 for Biomedical Purposes', *Coatings*, vol. 15, no. 5, p. 498, Apr. 2025, doi: 10.3390/coatings15050498.

[15] F. Simchen, M. Sieber, A. Kopp, and T. Lampke, 'Introduction to Plasma Electrolytic Oxidation—An Overview of the Process and Applications', *Coatings*, vol. 10, no. 7, p. 628, Jun. 2020, doi: 10.3390/coatings10070628.

[16] A. Jangde, S. Kumar, and C. Blawert, 'Role of glycerine on formation & corrosion characteristic of PEO layer formed over Mg alloy in a high-concentrated mixed silicate-phosphate-based electrolyte', *Surface and Coatings Technology*, vol. 450, p. 128971, Nov. 2022, doi: 10.1016/j.surfcoat.2022.128971.

[17] F. Witte, 'The history of biodegradable magnesium implants: A review☆', *Acta Biomaterialia*, vol. 6, no. 5, pp. 1680–1692, May 2010, doi: 10.1016/j.actbio.2010.02.028.

[18] G. Song and A. Atrens, 'Understanding Magnesium Corrosion—A Framework for Improved Alloy Performance', *Adv Eng Mater*, vol. 5, no. 12, pp. 837–858, Dec. 2003, doi: 10.1002/adem.200310405.
[19] Lide, D. R. (Ed.). CRC, *Handbook of Chemistry and Physics*, 85th edn.
[20] Y. Xin, T. Hu, and P. K. Chu, 'Influence of Test Solutions on In Vitro Studies of Biomedical Magnesium Alloys', *J. Electrochem. Soc.*, vol. 157, no. 7, p. C238, 2010, doi: 10.1149/1.3421651.
[21] M. B. Kannan, R. Walter, A. Yamamoto, H. Khakbaz, and C. Blawert, 'Electrochemical surface engineering of magnesium metal by plasma electrolytic oxidation and calcium phosphate deposition: biocompatibility and *in vitro* degradation studies', *RSC Adv.*, vol. 8, no. 51, pp. 29189–29200, 2018, doi: 10.1039/C8RA05278F.
[22] X. Lu *et al.*, 'Plasma electrolytic oxidation coatings with particle additions – A review', *Surface and Coatings Technology*, vol. 307, pp. 1165–1182, Dec. 2016, doi: 10.1016/j.surfcoat.2016.08.055.
[23] L. Chen *et al.*, 'Effects of fluoride on the proliferation and activation of osteoblasts by regulating methylation of the DNA repair genes MGMT and MLH1', *Regenerative Therapy*, vol. 19, pp. 107–112, Mar. 2022, doi: 10.1016/j.reth.2022.01.004.
[24] Z. Lujun, L. Hongzhan, M. Qingmei, L. Jiangbo, and L. Zhengxian, 'The mechanism for tuning the corrosion resistance and pore density of plasma electrolytic oxidation (PEO) coatings on Mg alloy with fluoride addition', *Journal of Magnesium and Alloys*, vol. 11, no. 8, pp. 2823–2832, Aug. 2023, doi: 10.1016/j.jma.2021.10.007.
[25] D. Saran, A. Kumar, S. Bathula, D. Klaumünzer, and K. K. Sahu, 'Review on the phosphate-based conversion coatings of magnesium and its alloys', *Int J Miner Metall Mater*, vol. 29, no. 7, pp. 1435–1452, Jul. 2022, doi: 10.1007/s12613-022-2419-2.
[26] M. A. Hafeez, A. Farooq, A. Zang, A. Saleem, and K. M. Deen, 'Phosphate chemical conversion coatings for magnesium alloys: a review', *J Coat Technol Res*, vol. 17, no. 4, pp. 827–849, Jul. 2020, doi: 10.1007/s11998-020-00335-2.
[27] S. Bagherifard, 'Mediating bone regeneration by means of drug eluting implants: From passive to smart strategies', *Materials Science and Engineering: C*, vol. 71, pp. 1241–1252, Feb. 2017, doi: 10.1016/j.msec.2016.11.011.
[28] A. Bordbar-Khiabani, B. Yarmand, S. Sharifi-Asl, and M. Mozafari, 'Improved corrosion performance of biodegradable magnesium in simulated inflammatory condition via drug-loaded plasma electrolytic oxidation coatings', *Materials Chemistry and Physics*, vol. 239, p. 122003, Jan. 2020, doi: 10.1016/j.matchemphys.2019.122003.
[29] E. Petrova *et al.*, 'Use of synergistic mixture of chelating agents for in situ LDH growth on the surface of PEO-treated AZ91', *Sci Rep*, vol. 10, no. 1, p. 8645, May 2020, doi: 10.1038/s41598-020-65396-0.
[30] B. Shi *et al.*, 'Advances in amelioration of plasma electrolytic oxidation coatings on biodegradable magnesium and alloys', *Heliyon*, vol. 10, no. 4, p. e24348, Feb. 2024, doi: 10.1016/j.heliyon.2024.e24348.
[31] Joseph I. Goldstein, Dale E. Newbury, Joseph R. Michael, Nicholas W. M. and Ritchie, John Henry J. Scott, and David C. Joy, *Scanning Electron Microscopy and X-Ray Microanalysis.*, 4th ed. New York, NY: Springer, 2018. doi: doi: 10.1007/978-1-4939-6676-9.
[32] *X-Ray Diffraction*. Springer, Singapore, 2025. doi: https://doi-org.ezproxy.biblio.polito.it/10.1007/978-981-97-2998-2_676.
[33] T. Pluskal, S. Castillo, A. Villar-Briones, and M. Orešič, 'MZmine 2: Modular framework for processing, visualizing, and analyzing mass spectrometry-based molecular profile data', *BMC Bioinformatics*, vol. 11, no. 1, p. 395, Dec. 2010, doi: 10.1186/1471-2105-11-395.
[34] L. Prince, X. Noirfalise, Y. Paint, and M. Olivier, 'Corrosion mechanisms of AZ31 magnesium alloy: Importance of starting pH and its evolution', *Materials & Corrosion*, vol. 73, no. 10, pp. 1615–1630, Oct. 2022, doi: 10.1002/maco.202213116.

[35] A. Ghasemi, V. S. Raja, C. Blawert, W. Dietzel, and K. U. Kainer, 'Study of the structure and corrosion behavior of PEO coatings on AM50 magnesium alloy by electrochemical impedance spectroscopy', *Surface and Coatings Technology*, vol. 202, no. 15, pp. 3513–3518, Apr. 2008, doi: 10.1016/j.surfcoat.2007.12.033.
[36] Organon LLC. (2022), 'betamethasone sodium phosphate and betamethasone acetate injectable suspension, USP – Prescribing information. Organon & Co.' Celestone® Soluspan®.
[37] 'Merck & Co., Inc. Celestone® Soluspan® (betamethasone sodium phosphate and betamethasone acetate) Injectable Suspension, USP – FDA Labeling.'
[38] 'Japanese Pharmacopoeia. Betamethasone Sodium Phosphate.' National Institutes of Health Sciences, Japan.
[39] S. Mansouri, X. D. Chen, and M. W. Woo, 'Design of micron-sized salt particles by ethanol vapour drying', *Powder Technology*, vol. 323, pp. 558–562, Jan. 2018, doi: 10.1016/j.powtec.2016.06.050.
[40] C. Liu, J. Liang, J. Zhou, Q. Li, and L. Wang, 'Characterization of AZ31 magnesium alloy by duplex process combining laser surface melting and plasma electrolytic oxidation', *Applied Surface Science*, vol. 382, pp. 47–55, Sep. 2016, doi: 10.1016/j.apsusc.2016.04.047.
[41] D. B. Verbeeck, R. M. H., 'Solubility of Magnesium Hydrogen Phosphate Trihydrate and Ion-Pair Formation in the System $Mg(OH)_2$–H_3PO_4–H_2O at 25 °C.', *Inorganic Chemistry, 23(13), 1922–1926.*, 1984, doi: https://doi.org/10.1021/ic00181a026.
[42] Y. Yang, J. Han, Y. Cui, and R. Liu, 'An investigation on hydration products of MKPC at low magnesium to phosphate ratio using XRD Rietveld Method', *Materials Letters*, vol. 361, p. 136096, Apr. 2024, doi: 10.1016/j.matlet.2024.136096.
[43] D. Liu, L. Mao, and H. Wang, 'Preparation of uniform newberyite crystal in nonaqueous system', *Materials Letters*, vol. 240, pp. 169–171, Apr. 2019, doi: 10.1016/j.matlet.2019.01.016.
[44] E. K. Brooks, S. Der, and M. T. Ehrensberger, 'Corrosion and mechanical performance of AZ91 exposed to simulated inflammatory conditions', *Materials Science and Engineering: C*, vol. 60, pp. 427–436, Mar. 2016, doi: 10.1016/j.msec.2015.11.059.
[45] U. Malayoglu, K. C. Tekin, and S. Shrestha, 'Influence of post-treatment on the corrosion resistance of PEO coated AM50B and AM60B Mg alloys', *Surface and Coatings Technology*, vol. 205, no. 6, pp. 1793–1798, Dec. 2010, doi: 10.1016/j.surfcoat.2010.08.022.
[46] N. V. Phuong, B. R. Fazal, and S. Moon, 'Cerium- and phosphate-based sealing treatments of PEO coated AZ31 Mg alloy', *Surface and Coatings Technology*, vol. 309, pp. 86–95, Jan. 2017, doi: 10.1016/j.surfcoat.2016.11.055.
[47] Y.-B. Li *et al.*, 'Effect of Reaction Temperature on the Microstructure and Properties of Magnesium Phosphate Chemical Conversion Coatings on Titanium', *Molecules*, vol. 28, no. 11, p. 4495, Jun. 2023, doi: 10.3390/molecules28114495.

Use of Artificial Intelligence Tools

Artificial intelligence (AI)-based tools were used during the preparation of this thesis mainly as a support for language revision, translation, and text fluidification. AI was employed to improve the clarity, readability, and grammatical correctness of the written content, as well as to verify the coherence and completeness of the presented information. In some cases, AI tools were also used as a preliminary support for identifying missing information, suggesting possible scientific interpretations, and assisting in the search for relevant literature references. Nevertheless, all experimental activities, data analyses, interpretations, and final evaluations were critically reviewed and validated by the author.